ACS OMEGA

Open Access

http://pubs.acs.org/journal/acsodf

Article

Study on the Efficacy and Potential Mechanism of Topical Shen Bai Hair Growing Decoction against Androgenetic Alopecia Based on Ultrahigh Performance Liquid Chromatography Quadrupole Time-of-Flight Mass Spectrometry and RNA-seq

Mingxi Li, Xiujun Zhang, Yan Wang,* Beibei Xiang,* Zhaoyi Liu, Wenwen Zhang, Xuanming Liu, and Ruoxi Guo

Cite This: *ACS Omega* 2024, 9, 10834−10851

Read Online

ACCESS | Metrics & More | Article Recommendations

ABSTRACT: Androgenetic alopecia (AGA) is a major problem that can happen to people of all ages, leading to psychological problems, such as anxiety and depression. Topical Shen Bai hair growing decoction (TSBHGD) is based on the pathogenesis of AGA, combined with Traditional Chinese Medicine theory, improved by the Tianjin Academy of Traditional Chinese Medicine Affiliated Hospital according to its clinical treatment experience. This study was designed to demonstrate the therapeutic efficacy of TSBHGD against AGA, analyze the chemical components of TSBHGD as well as the skin-retained and blood-retained components in mice after topical administration of TSBHGD, and clarify the mechanism of its therapeutic efficacy. It was demonstrated that TSBHGD could suppress TNF-α and IL-6 levels and improve pathological phenomena such as hair loss, reduced follicle density, and dermal thickness caused by testosterone solution. Totally 35 components were identified in TSBHGD extracts, 12 skin-retained components were identified in drug-containing skin, and 7 blood-retained components were identified in drug-containing plasma, according to ultrahigh performance liquid chromatography quadrupole time-of-flight mass spectrometry. Transcriptomic sequencing revealed that some of the genes in AGA mice had altered expression patterns, which could be reversed by TSBHGD. Through network pharmacology analysis, it was found that TSBHGD mainly regulated eight signaling pathways, among which the apoptosis signaling pathway ranked first with a significance of 0.00149. Finally, both Bcl-2 and Caspase family proteins in the apoptosis signaling pathway were examined by Western blot. It was confirmed that TSBHGD could inhibit the apoptosis level in AGA mice's skin tissue to exert an anti-AGA effect. This will facilitate the development of new-generation herbal compound formulas with precise efficacy and provide novel ideas for AGA therapy.

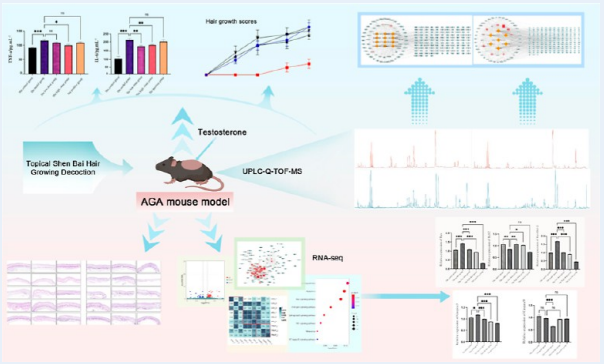

1. INTRODUCTION

Androgenetic alopecia (AGA) represents a prevalent pattern of hair loss in both males and females. It is described as a shortening of the hair growth cycle and a gradual shrinking of hair follicles, ultimately resulting in an overall reduction in the hair count.[1] Clinically, AGA stands as the predominant form of hair loss, representing a substantial 84.8% of all cases of alopecia,[2] and in China, the incidence of AGA is reported as 21.3% among males and 6.0% among females.[3] Concurrently, various investigations indicate that within Caucasian males, the likelihood of developing AGA reaches approximately 30% before age 30, escalates to 50% before age 50, and surges to 80% before age 70. In contrast, among Caucasian females, the prevalence of AGA ranges from 3 to 12% before age 30 and from 14 to 28% before age 60, which suggests that AGA incidence will gradually increase with age.[4] Clinical manifestations include the presence of a smooth, hairless surface within the alopecia region along with greasy hair, dandruff, and pruritus. Furthermore, hair thinning progressively develops in the frontotemporal lobe area and crown of the head, eventually leading to baldness.[5] This condition can seriously affect the patient's daily interpersonal interaction and social confidence, leading to psychological problems such as anxiety and depression.[6]

Received: December 7, 2023
Revised: February 8, 2024
Accepted: February 14, 2024
Published: February 26, 2024

AGA management encompasses a spectrum of therapeutic approaches, including pharmaceutical interventions, low-level laser therapy, hair transplantation procedures, photobiomodulation techniques, as well as Traditional Chinese Medicine (TCM) treatments.[7] Presently, the US Food and Drug Administration (FDA) has approved exclusively topical minoxidil and oral finasteride as treatments for AGA.[8] Although the specific mechanism of minoxidil is unclear, this drug has been found to have significant undesirable dermatological effects, including facial hypertrichosis, contact dermatitis, erythema, redness, scalp dryness, and dandruff.[9] Finasteride has also been found to cause different side effects, including menstrual irregularity and breast enlargement or tenderness in females, as well as decreased libido and erectile dysfunction in males.[10] Besides, hair loss will continue once the medication is discontinued, while both drugs have questionable effectiveness and safety. Therefore, exploring safe and effective TCM to replace conventional therapies for AGA has been of great social and clinical importance in recent years.[11]

Hair loss has been a subject of study in TCM for millennia, and many classic herbal compound formulas have been widely used in AGA treatment. According to TCM theory, hair growth is intricately linked to the cyclical fluctuations of vital essence and blood within the kidneys, as well as the nourishment of qi and blood, and classifies hair loss into the following four main syndrome types: (i) dampness and heat in the spleen and stomach; (ii) blood-heat and wind-dryness; (iii) blood deficiency and wind-dryness; (iv) liver and kidney deficiency. The respective therapeutic approaches can be succinctly outlined as follows: stimulating the spleen and inducing dampness; cooling blood and moistening dryness; nourishing blood and dispelling wind; and nourishing the liver and kidneys.[12] In China, numerous TCMs have been employed to enhance blood circulation, nourish the liver and kidneys, clear heat, and remove toxicity.[13] Modern medicine has found that Chinese herbal drugs can mitigate hair loss by modulating hair growth factors and inhibiting apoptosis, with the benefit of fewer side effects and significant results.[14] The Leaves of *Platycladus orientalis* (L.) Franco is a traditional herbal remedy for hair loss by cooling the blood, stopping bleeding, blackening hair, and promoting hair growth.[15] It has also been shown to have an inhibitory effect on the (5-alpha-reductase) 5-AR enzyme.[16] The rhizome of *Ligusticum chuanxiong Hort* can stimulate blood circulation and hair follicle growth.[17] Moreover, Ginseng and its major bioactive components have been proven to modulate the expression of key proteins associated with the hair growth cycle phases, which can stimulate hair growth while averting hair loss.[18] Other herbs such as ginger have the potential to improve the balance between oxidation and antioxidation within erythrocytes and lymphocytes, thereby restoring serum zinc levels to physiological norms.[19] Topical Shen Bai hair growing decoction (TSBHGD) is a compounded Chinese medicinal preparation based on TCM theory and clinical treatment experience. It regulates qi and blood, relieving depression and nourishing the liver and kidneys, and has been studied for safety at an early stage.

This study was designed to assess hair growth-promoting potential and underlying mechanisms of TSBHGD in the AGA mouse model suppressed by testosterone. The main chemical components of TSBHGD retained in skin and blood were identified by ultrahigh performance liquid chromatography quadrupole time-of-flight mass spectrometry (UPLC-Q-TOF-MS) and potential mechanisms were identified by RNA sequencing (RNA-seq) and Western Blot analysis. This research endeavors to establish a theoretical foundation for the clinical application of TCM in alopecia treatment and provide novel insights into the investigation of active components derived from Chinese herbal drugs and further the theoretical advancements in the modernization of TCM.

2. MATERIALS AND METHODS

2.1. Materials and Reagents. Testosterone propionate (TP; 25 mg/mL) was purchased from Hangzhou Animal Medicine Factory (Hangzhou, China). Minoxidil (5%) was purchased from Zhejiang Wansheng Pharmaceutical Co., Ltd. (Hangzhou, China). Enzyme-linked immunosorbent assay (ELISA) kits for mouse TNF-α and mouse IL-6 were purchased from R&D Systems (MN, USA). Antibodies for Caspase-3, Caspase-9, Bcl-2, Bax, and goat antirabbit IgG were purchased from Cell Signaling Technology (MA, USA). Unless otherwise noted, all other reagents used in this study were of analytical grade and purchased from Beijing Solarbio Science & Technology Co., Ltd. (Beijing, China).

Table 1. Prescription for Topical TSBHGD

botanical name	family	part used	local name	quantity (g)
Salvia miltiorrhiza Bge.	Lamiaceae	radix and rhizoma	Dan Shen	200
Ligusticum chuanxiong Hort.	Apiaceae	rhizoma	Chuan Xiong	100
Platycladus orientalis (L.)Franco	Cupressaceae	leaf	Ce Bai Ye	200
Cyperus rotundus L.	Cyperaceae	rhizoma	Xiang Fu	200
Panax ginseng C. A. Mey.	Araliaceae	radix and rhizoma	Hong Shen	200
Zanthoxylum bungeanum Maxim.	Rutaceae	pericarp	Hua Jiao	50
Zingiber officinale Rosc.	Zingiberaceae	rhizoma	Gan Jiang	50

Table 2. Gel System for Topical TSBHGD

compositions	quantity (% W/W)
Carbomer 940	1.8
Glycerin	10.0
propylene glycol	20.0
Laurocapram	1.0
hyaluronic acid	0.2
herbal complex extract	50.0
Triethanolamine	qs
Phenoxyethanol	0.5
distilled water	ad 100

2.2. Preparation of Plant Extracts and Topical Agents. The TCMs used in this experiment, as shown in Table 1, were provided by the Tianjin University of Traditional Chinese Medicine (Tianjin, China). Voucher specimens were stored at the College of Traditional Chinese Medicine, Tianjin University of Traditional Chinese Medicine. All raw drugs were powdered and extracted twice with the heating reflux method 8 times v/w of 70% ethanol for 2 h each time. The extraction was filtered through filter paper and concentrated to 4 g/mL with a rotary evaporator. The formulation of TSBHGD is given in Table 2. The carbomer 940 and glycerin were mixed and dispersed in a small quantity of distilled water,

https://doi.org/10.1021/acsomega.3c09648
ACS Omega 2024, 9, 10834−10851

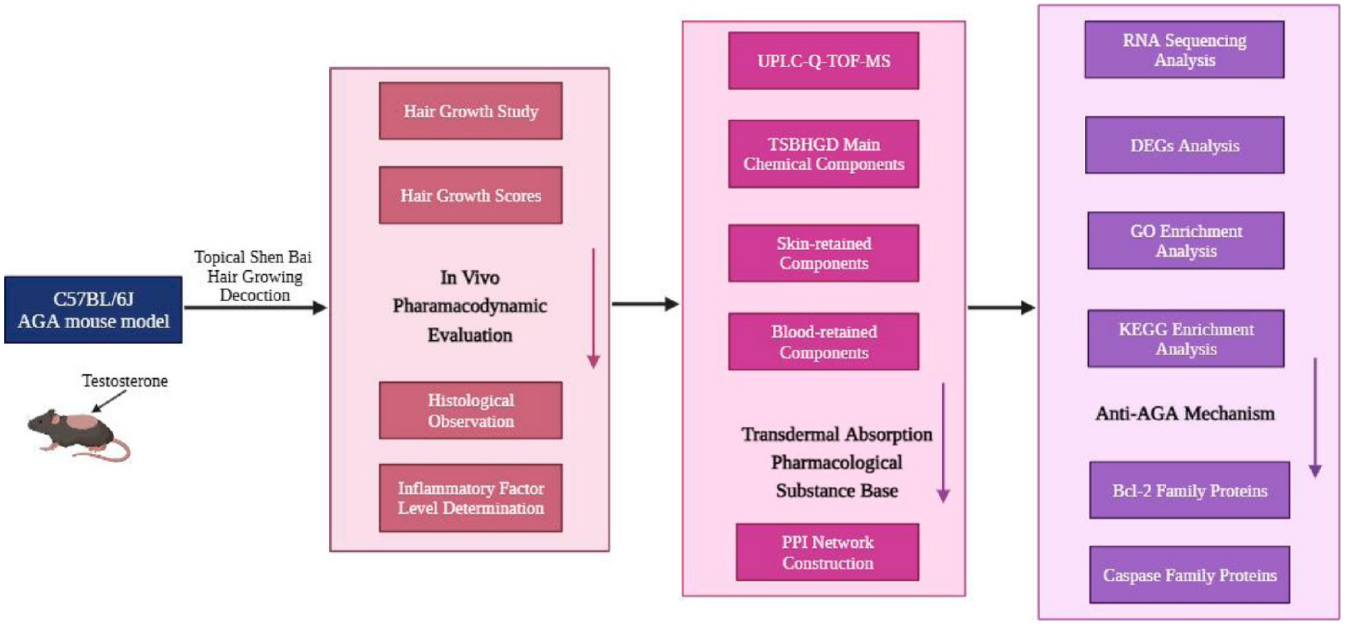

Figure 1. Experimental flowchart.

followed by the addition of propylene glycol, laurocapram, hyaluronic acid, herbal complex extract, and phenoxyethanol under constant stirring. To achieve the desired skin pH (6.5), triethanolamine was added to the mixture. Finally, the volumes of the formulation were fixed at 100 mL with the addition of distilled water.

2.3. Animals and Treatments. Fifty male C57BL/6J mice (6 weeks old, 18−22 g) were provided by Beijing Vital River Laboratory Animal Technology Co., Ltd. (Beijing, China). Animals were placed in an air-conditioned room (23 ± 3 °C, 35−60%, 12:12 h light/dark cycles). All animals received free feed and water during the experiment. All experimental procedures, animal care, and processing were carried out in accordance with the guidelines provided in the national standard "Requirements for the Environment and Housing Facilities of Laboratory Animals" (GB 14925-2010). Also, this experiment was approved by the Committee on Animal Research and Ethics of Tianjin University of Traditional Chinese Medicine (approval no. TCM-LAEC2022048). The animals were randomly divided into five groups of ten mice each after 1 week of adaptation. The dorsal hairs of mice in an area of 2 cm × 2 cm were gently depilated with a depilatory cream. Groups were treated as follows: (A) a control group (did not receive testosterone); (B) a model group (only testosterone treated); (C) a TSBHGD low-dose group (testosterone + TSBHGD low-dose treated); (D) a TSBHGD high-dose group (testosterone + TSBHGD high-dose treated); and (E) a positive group (testosterone + minoxidil treated). Except for the control group, all groups received a topical application of 0.2% (w/v) testosterone solution on the shaved back at a dose of 10 mg/kg daily in three equal parts for 14 consecutive days (9:00, 13:00, and 17:00) to establish the AGA mouse model. After topical testosterone application for 30 min, 1 mL of the appropriate drug solution was topically administered as follows: the TSBHGD low-dose group received 1 g/mL hair-growing decoction, the TSBHGD high-dose group received 2 g/mL hair-growing decoction, the positive group received 2.5 mg/mL minoxidil, and the control and model groups received a blank substrate as control.

2.4. Hair Growth Study. *2.4.1. Hair Regrowth in AGA Mice.* Hair regrowth and skin color in each group's depilated area were evaluated by daily visual observations. Photographs of the mice's dorsal skin were taken on days 0, 7, and 14 after starting the treatment. The hair regrowth was evaluated in each mouse on days 0, 4, 7, 11, and 14 by scoring hair growth and skin color from 0 to 3. The evaluation criteria were as follows: score 0 = the dorsal skin is pink and no growth observed; 1 = the dorsal skin is gray and less than 10% growth; 2 = the dorsal skin is black and less than 50% growth; 3 = the dorsal skin is black and 70% to full growth observed. Meanwhile, gently pull the new hairs three times with the thumb and index finger; if over 10% of the new hairs are removed, the hair pull test is positive and minus 0.5 points.

2.4.2. Histological Determination. Animals were executed on days 0, 7, and 14 after depilation, a 1 cm × 1 cm of dorsal skin was excised, fixed in 4% paraformaldehyde, and embedded in paraffin blocks to obtain suitable sections. Sections were processed for hematoxylin and eosin (H&E) staining and analyzed by a light microscope. The longitudinal sections were prepared for overall histological assessment, while transverse sections were performed to determine hair follicle counts in the anagen and telogen phases.

2.4.3. Determination of TNF-α and IL-6 Levels by ELISA Analysis. Blood samples were obtained from each group of C57BL/6J mice by directly accessing the postocular venous plexus. These samples were left to coagulate at room temperature for 30 min and then subjected to centrifugation at 4 °C and 3000 rpm for 15 min to separate the serum. Following this, TNF-α and IL-6 levels were quantified using ELISA kits according to the manufacturer's guidelines.

2.5. UPLC-Q-TOF-MS Analysis. *2.5.1. Sample Preparation.* Blood samples were collected from mice under 1.25% tribromoethanol anesthesia in ethylenediaminetetraacetic acid (EDTA) tubes, the mice were executed immediately after sample collection, and dorsal skin samples were taken from mice. EDTA-treated blood was centrifuged at 4 °C and 4000 rpm for 10 min to obtain plasma samples. Then, the collected plasma samples were vortexed with triple methanol for 3 min.

https://doi.org/10.1021/acsomega.3c09648
ACS Omega 2024, 9, 10834−10851

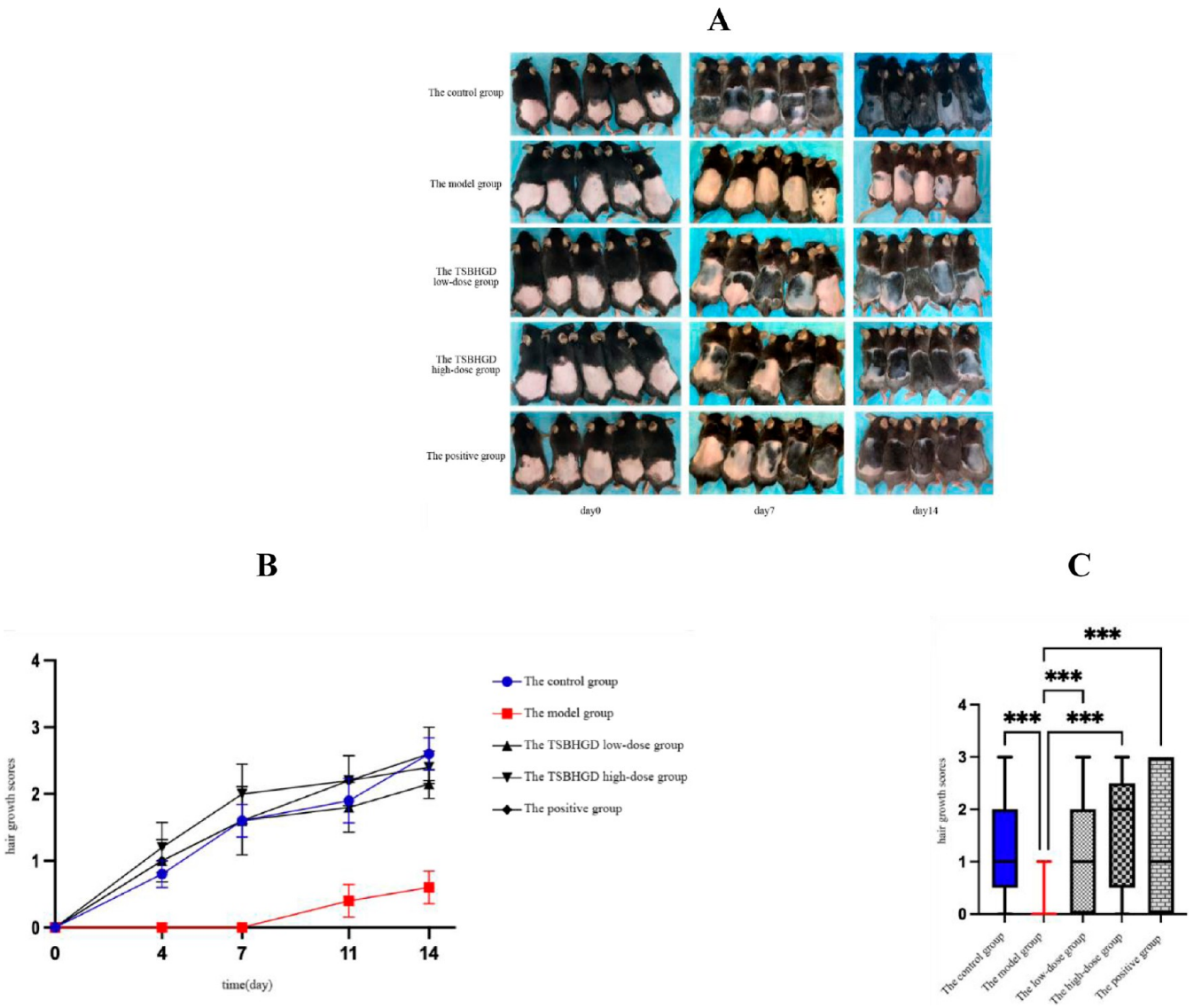

Figure 2. Hair regenerative effects of TSBHGD in a testosterone-induced AGA mouse model. (A) Photographs of hair removal areas were taken on days 0, 7, and 14 after treatment. (B) Hair growth scores were measured on days 0, 4, 7, 11, and 14 after treatment. (C) Statistical test of hair growth scores for each group.

Meanwhile, skin samples were washed three times with sterile saline to wash away the unabsorbed drug components in the epidermis, then vortexed with quintuple methanol for 3 min, and homogenized at −50 °C for 10 min in a frozen high-throughput tissue grinder. Plasma and tissue samples were both centrifuged at 4 °C and 12 000 rmp for 10 min, following the transfer of supernatants into fresh tubes, respectively. Next, the residues were subjected to evaporation until dryness under a soft nitrogen stream, redissolution in 100 μL 70% methanol, vortex-mixed for 3 min, ultrasound treatment for 10 min, and centrifuged at 4 °C, 12 000 rmp for 15 min to obtain supernatants for subsequent analysis using UPLC-Q-TOF-MS.

2.5.2. Mass Spectrometric Conditions. Chromatographic analysis was conducted using the Waters Acquity UPLC System, coupled to a Q-TOF mass spectrometer (Waters, USA). An Acquity UPLC BEH C_{18} Column (2.1 × 100 mm, 1.7 μm) was used to separate the components. The column temperature was maintained at 50 °C. Formic acid 0.1% in methanol (eluent A) and formic acid 0.1% in water (eluent B) were used as a solvent with a flow rate of 0.3 mL/min. The gradient elution schedule was as follows: 5 to 30% A at 0−11 min, 30 to 35% A at 11−20 min, 35 to 38% A at 20−26 min, 38 to 38% A at 26−30 min, 38 to 42% A at 30−33 min, 42 to 51% A at 33−40 min, 51 to 75% A at 40−46 min, 75 to 100% A at 46−48 min, and 100 to 100% A at 48−50 min with 1 μL sample injection volume.

The chemical component was carried out using Q-TOF mass spectrometry coupled to an electrospray ionization interface (ESI). The ESI source operated in both positive and negative ion modes between m/z 50 and 1200 with a full scan and optimization parameters: cone voltage 40 V, source temperature 120 °C, desolvation temperature 450 °C, cone gas flow 50 L/h, desolvation gas flow 800 L/h, and the capillary voltage of 3 kV (ESI^+) or 3 kV (ESI^-). The acquisition and processing of all data were performed using MassLynx (V4.1; Waters, USA).

2.5.3. Protein−protein Interaction Network Construction. The molecular weight information and SMILES standard format of skin-retained and blood-retained components were searched using the PubChem database (https://pubchem.ncbi.

https://doi.org/10.1021/acsomega.3c09648
ACS Omega 2024, 9, 10834−10851

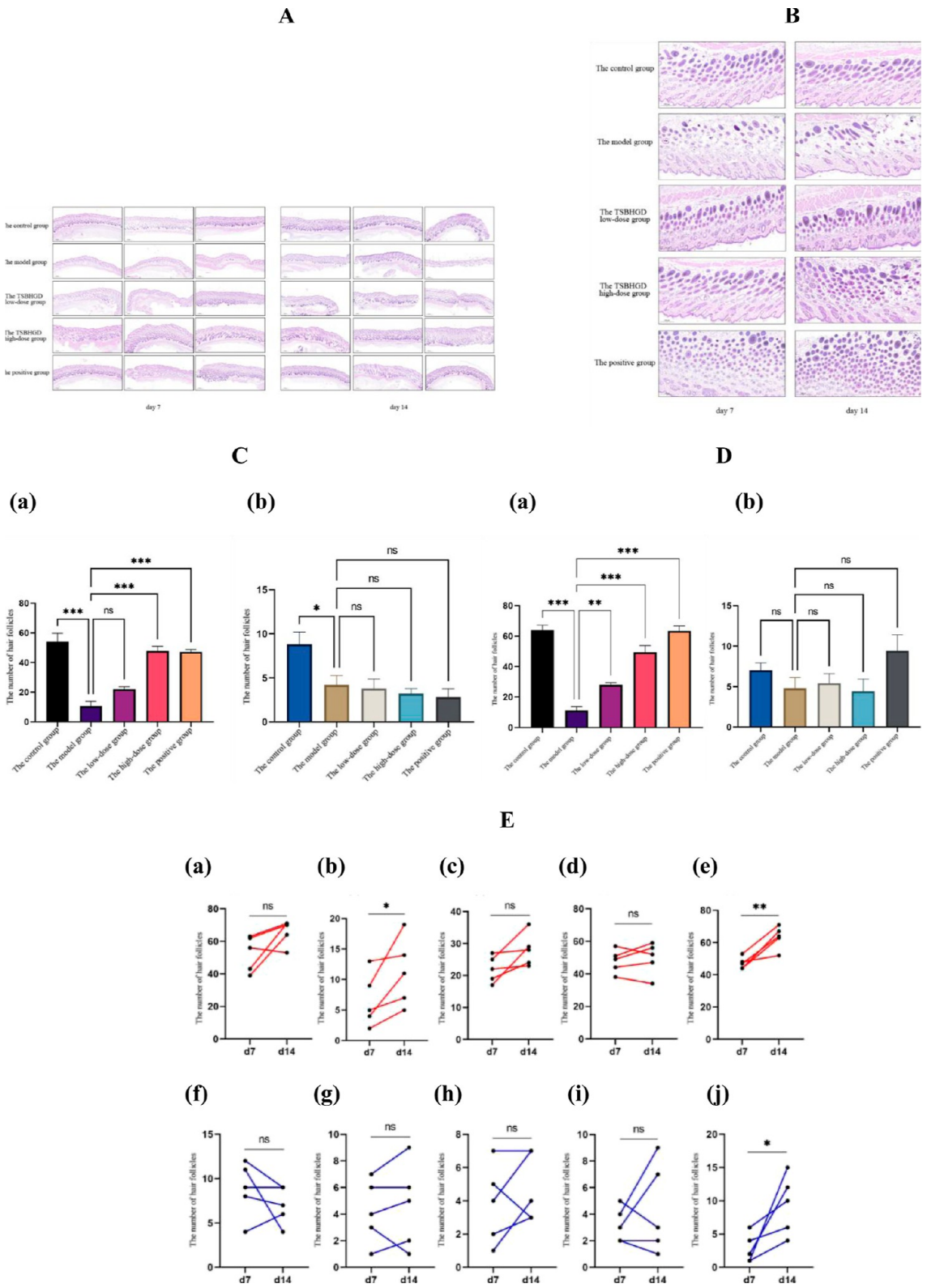

Figure 3. Histological differences and hair follicle counts of skin in hair removal areas during days 7 and 14 after treatment. (A) Histopathological changes of skin in hair removal areas (30×). (B) Histopathological changes of skin in hair removal areas (100×). (C) Number of hair follicles in hair removal areas on day 7 (a: anagen, b: telogen). (D) Number of hair follicles in hair removal areas on day 14 (a: anagen, b: telogen). (E) Changes in the number of anagen follicles (a−e) and telogen follicles (f−j) between days 7 and 14. (a/f: Control, b/g: Model, c/h: Low-dose TSBHGD, d/i: High-dose TSBHGD, e/j: Positive).

nlm.nih.gov/). Then, Swiss Target Prediction (http://www.swisstargetprediction.ch/) was used to predict the potential targets and screen out targets with "probability (>0.10)". The STRING database (https://string-db.org/) was used for interaction analysis on human-derived targets of skin-retained and blood-retained components, with the species-genus set as "

https://doi.org/10.1021/acsomega.3c09648
ACS Omega 2024, 9, 10834−10851

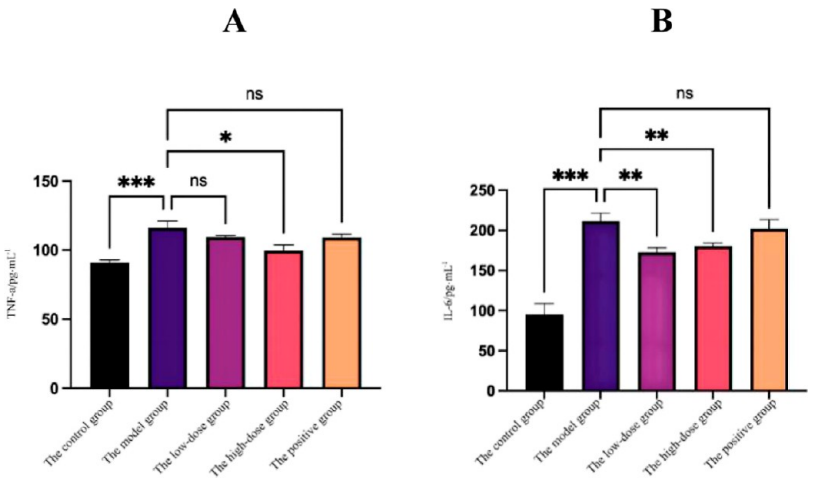

Figure 4. Effects of TSBHGD on the inhibition of inflammation in mice. (A) Effect of TSBHGD on the TNF-α level on day 14 after treatment. (B) Effect of TSBHGD on the IL-6 level on day 14 after treatment.

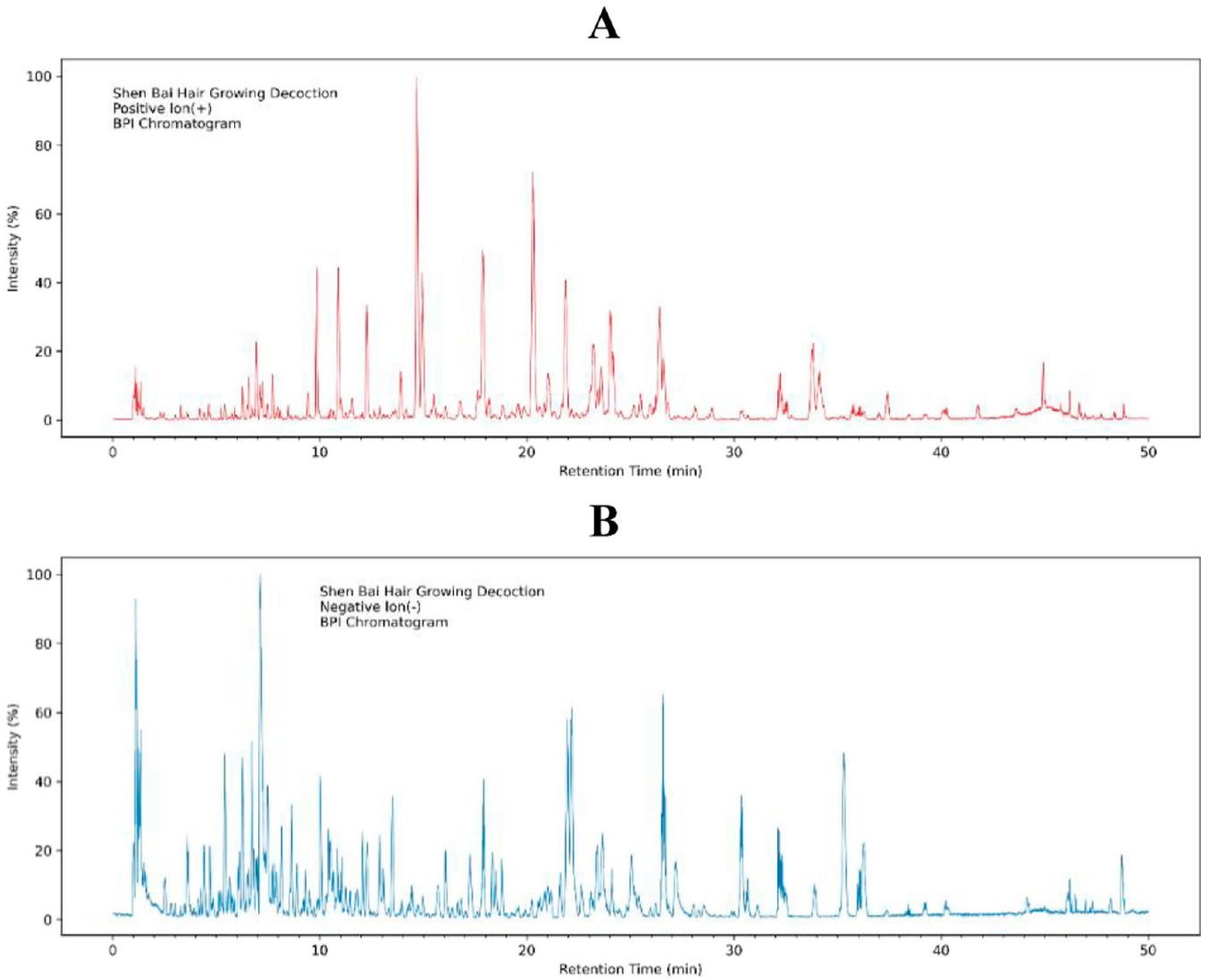

Figure 5. BPI chromatograms of TSBHGD extracts. (A) BPI chromatogram of TSBHGD extracts in positive ion mode. (B) BPI chromatogram of TSBHGD extracts in negative ion mode.

Homo sapiens". Cytoscape V3.7.2 software (http://manual.cytoscape.org/en/stable/) and "R package: clusterProfiler" were used to set up a protein−protein interactions (PPI) network.

https://doi.org/10.1021/acsomega.3c09648
ACS Omega 2024, 9, 10834−10851

Table 3. Component Identification of TSBHGD Extracts in Positive and Negative Ion Modes

peak (no.)	ion mode	R_t (min)	components name	molecular formula	measured mass (no.)	calculated mass (no.)	error (ppm)	MS/MS
1	[M − H]+	1.203	butylidenephthalide	$C_{12}H_{12}O_2$	189.0916	189.0902	−2.1	89.4471
2	[M − H]+	7.329	trijuganone C	$C_{20}H_{20}O_5$	341.1389	341.1399	−1.6	171.0734, 114.3848, 86.0406
3	[M − H]+	9.781	senkyunolide H	$C_{12}H_{16}O_4$	225.1127	225.1119	−3.1	207.4182, 189.4428
4	[M − H]+	12.331	miltirone	$C_{19}H_{22}O_2$	283.1698	283.1684	−1.5	142.0888, 95.0618, 71.5483
5	[M − H]+	14.991	tanshinone IIA	$C_{19}H_{18}O_3$	295.1334	295.1345	1.9	277.1919, 249.3549
6	[M − H]+	17.813	methylenetanshinquinone	$C_{18}H_{14}O_3$	279.1021	279.1025	0.3	140.0550, 93.7059, 70.5314
7	[M − H]+	20.327	tanshinone IIB	$C_{19}H_{18}O_4$	311.1283	311.1285	−0.9	156.0681, 104.3813, 78.5380
8	[M − H]+	21.866	senkyunolide A	$C_{12}H_{16}O_2$	193.1229	193.0388	−0.2	91.4061
9	[M − H]+	24.349	butylphthalide	$C_{12}H_{14}O_2$	191.1072	191.6543	0.6	145.7898
10	[M − H]+	26.926	dihydrotanshinone I	$C_{18}H_{14}O_3$	279.1021	270.1005	−2.4	261.8266, 233.3103
11	[M − H]+	34.470	levistilide A	$C_{24}H_{28}O_4$	381.2066	381.2048	−3.9	191.7542
12	[M − H]−	1.311	danshensu	$C_9H_{10}O_5$	197.0450	197.0237	−1.4	179.9529, 137.1770
13	[M − H]−	5.795	caffeic acid	$C_9H_8O_4$	179.0344	179.0351	−1.1	135.1927, 117.5022, 107.8723
14	[M − H]−	6.688	quinic acid	$C_7H_{12}O_6$	191.0556	191.0552	0.7	173.1321, 155.5332, 137.4562, 127.5325
15	[M − H]−	7.781	apigenin	$C_{15}H_{10}O_5$	269.0450	269.0452	−1.4	241.5682, 221.5315, 117.4576, 107.9679
16	[M − H]−	8.698	epicatechin	$C_{15}H_{14}O_6$	289.0712	289.0707	−1.2	245.1667, 203.7458, 151.1237, 109.4235
17	[M − H]−	8.848	kaempferide	$C_{16}H_{12}O_6$	299.0556	299.0544	1.8	284.6238, 151.2303
18	[M − H]−	10.103	salvianolic acid F	$C_{17}H_{14}O_6$	313.0712	313.0727	1.9	269.2354, 159.7892
19	[M − H]−	12.087	salvianolic acid G	$C_{18}H_{12}O_7$	339.0505	339.0507	−2.7	169.0213, 112.3449, 84.0068
20	[M − H]−	13.566	chlorogenic acid	$C_{16}H_{18}O_9$	353.0873	353.0827	−1.0	191.5323, 208.1231
21	[M − H]−	16.136	rosmarinic acid	$C_{18}H_{16}O_8$	359.0767	359.0761	1.5	197.4234, 179.5231, 161.4564
22	[M − H]−	17.949	salvianolic acid D	$C_{20}H_{18}O_{10}$	417.0822	417.0828	−0.7	373.9879, 297.1467, 255.5734
23	[M − H]−	21.950	apigenin-7-*O*-beta-D-glucoside	$C_{21}H_{20}O_{10}$	431.0978	431.0976	−0.6	341.2379, 311.4523, 269.0789
24	[M − H]−	22.157	kaempferol-3-*O*-rhamnoside	$C_{21}H_{20}O_{10}$	431.0978	431.0942	−1.5	285.5245, 277.7645, 255.0122
25	[M − H]−	23.582	quercetin	$C_{15}H_{10}O_7$	301.0348	301.0340	−1.1	273.0396, 178.7645, 151.0232
26	[M − H]−	23.855	salvianolic acid C	$C_{26}H_{20}O_{10}$	491.0978	491.1216	0.7	245.0450, 163.0274, 122.0186
27	[M − H]−	24.097	salvianolic acid A	$C_{26}H_{22}O_{10}$	493.1135	493.1142	−0.3	313.8273, 295.8921
28	[M − H]−	25.022	amentoflavone	$C_{30}H_{18}O_{10}$	537.0822	537.0828	−1.9	443.7832, 417.5301, 375.8928, 331.0233, 203.3428
29	[M − H]−	26.812	monomethyllithospermate	$C_{28}H_{24}O_{12}$	551.1190	551.1171	1.1	275.0556, 183.0344, 137.0239
30	[M − H]−	27.372	myricetrin	$C_{15}H_{10}O_8$	463.0877	463.0882	−0.2	317.2620, 287.2324, 178.6456, 151.2356
31	[M − H]−	30.232	salvianolic acid B	$C_{36}H_{30}O_{16}$	717.1456	717.1449	0.4	537.1239, 321.8621
32	[M − H]−	30.684	dimethyllithospermate B	$C_{38}H_{34}O_{16}$	745.1769	745.1773	−0.5	372.0845, 247.7204, 185.5383
33	[M − H]−	32.271	ginsenoside Rg1	$C_{42}H_{72}O_{14}$	799.4844	799.4824	−1.9	637.6349, 475.0623
34	[M − H]−	35.308	ginsenoside Re	$C_{48}H_{82}O_{18}$	945.5423	945.5410	0.6	799.0245, 783.7827, 765.8762, 637.1023, 619.7992, 475.1982
35	[M − H]−	36.471	ginsenoside Rb1	$C_{54}H_{92}O_{23}$	1107.5951	1107.5949	1.7	945.1092, 783.1983, 621.5793

2.6. Bioinformatic Analysis and Experimental Verification. *2.6.1. RNA Sequencing Analysis.* For RNA-seq, library construction was performed by Guangzhou Kidio Biotechnology Co., Ltd. using the Illumina NovaSeq 6000 System. Fastp V0.18.0 was used to remove adapter sequences and low-quality base sequences (Q-value ≤20), and the remaining base sequences were compared and annotated to the mouse reference genome (GRCm39, NCBI) with the Hisat2 program. The expression counts for each sample were obtained using the FeatureCounts program, and the gene expression matrix was standardized by the FPKM method. Finally, the differentially expressed genes (DEGs) were filtered based on | fold change | ≥ 1.5 and | false discovery rate | ≤ 0.05 using the DESeq2 tool. Pearson's correlation coefficient was calculated using R V4.0.5 software to estimate the stability and operational correlation of the experimental results, and principal component analysis (PCA) was executed to uncover the structure or relationship among the samples, with the results visualized separately.

2.6.2. Functional Enrichment Analysis of Core Targets. Next, intersection targets were analyzed for Gene Ontology (GO) enrichment analysis of biological process (BP), cellular component (CC), and molecular function (MF) using the Metascape database (http://metascape.org/gp/index.html). Kyoto Encyclopedia of Genes and Genomes (KEGG) signaling pathway enrichment analysis was performed using the same database to identify potential biological pathways and functions associated with the targets. Various bioinformatic analyses were performed using R V4.0.5 software, with the adjusted P-value <0.01 and Q-value ≤0.05 set in the programming language.

2.7. Western Blot Analysis. Dorsal skin samples from C57BL/6J mice were promptly frozen in liquid nitrogen, ground to powder, homogenized in RIPA lysis buffer, and centrifuged at 4 °C and 12 000 rpm for 10 min to obtain

https://doi.org/10.1021/acsomega.3c09648
ACS Omega 2024, 9, 10834−10851

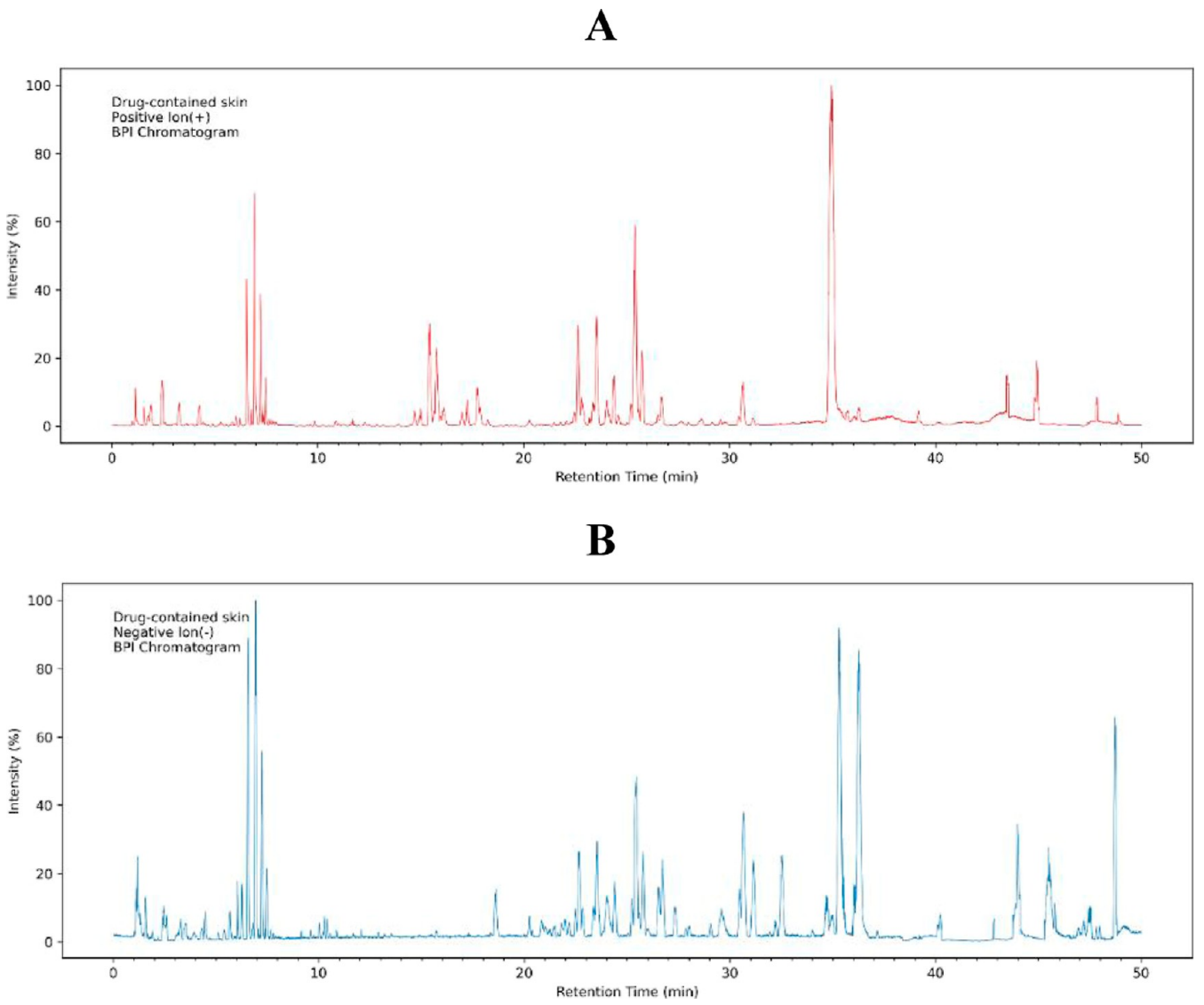

Figure 6. BPI chromatograms of drug-contained skin. (A) BPI chromatogram of drug-containing skin in positive ion mode. (B) BPI chromatogram of drug-contained skin in negative ion mode.

supernatants. Tissue lysates containing equal-mount proteins were segregated with 4−12% SDS-PAGE gels and transferred to PVDF membranes. After blocking with 5% skimmed milk for 1.5 h, the membranes were subjected to five washes with TBST and incubated with primary antibodies (1:2000 dilution) overnight at 4 °C. Next, after washing five times with TBST, the membranes were incubated with goat antirabbit IgG (1:10 000 dilution) at room temperature for 1 h. Immunoreactive signals were visualized and captured using enhanced chemiluminescence reagents, and the grayscale analysis of protein bands was analyzed using ImageJ V6.0 software.

2.8. Statistical Analysis. All statistical analyses of data from our experiments were performed using R V4.0.5 software. Results were presented as the mean ± standard deviation. Statistical analyses were performed using Student's *t*-test to determine significant differences between treatments. A *P*-value <0.05 was considered significant and each experiment was repeated at least three times (see Figure 1).

3. RESULT

3.1. Hair Growth Status and Hair Growth Scores. A testosterone-induced AGA mouse model was generated to validate the antialopecia effect of TSBHGD. Skin pigmentation serves as an indicator of hair growth, which is pink during the telogen phase and turns gray/black during the anagen phase. After 1 week of hair removal, the dorsal skin turned pink with some new hair visible in the control group, while the model group was without new hair visible. Mice treated with TSBHGD showed gray dorsal skin with some new hair growth, indicating that melanin was being produced and gradually accumulated in the dermis. The positive group showed the same hair growth as the TSBHGD groups, but there was visible hair loss. After 2 weeks of hair removal, the dorsal skin turned black and new hairs were visible in the control group, demonstrating that the hair follicles were entering the anagen phase. Part of the dorsal skin turned gray, but no significant hair growth was observed in the model group. Mice treated with TSBHGD showed remarkable patchy hair growth in the dorsal skin with nearly complete recovery of skin color, especially in the high-dose group. Significant patchy

https://doi.org/10.1021/acsomega.3c09648
ACS Omega 2024, 9, 10834−10851

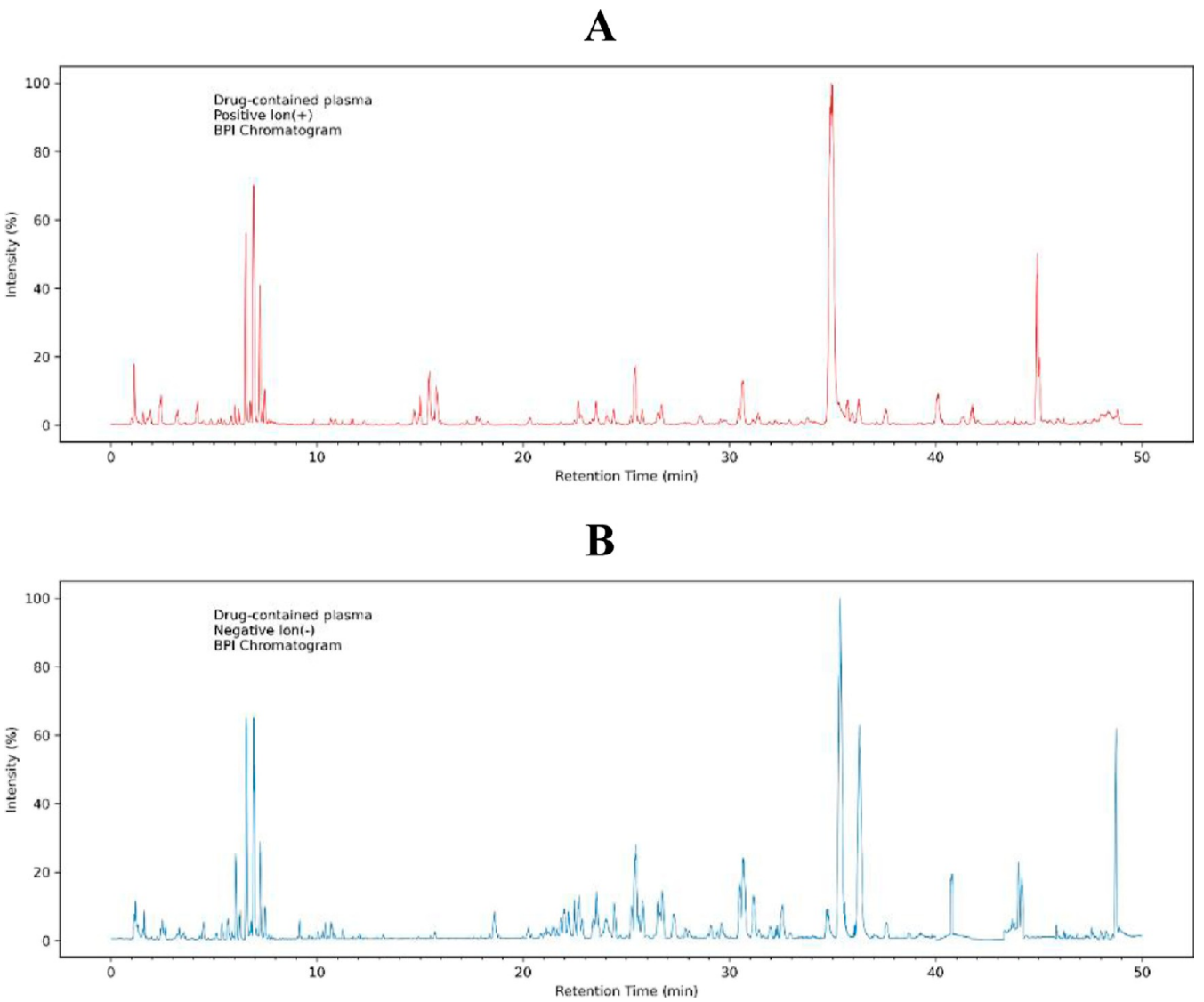

Figure 7. BPI chromatograms of drug-contained plasma. (A) BPI chromatogram of drug-containing plasma in positive ion mode. (B) BPI chromatogram of drug-contained plasma in negative ion mode.

Table 4. Compound Identification of Drug-Containing Skin in Positive and Negative Ion Modes

peak (no.)	ion mode	R_t (min)	components name	molecular formula	measured mass (no.)	calculated mass (no.)	error (ppm)	MS/MS
1	$[M-H]+$	1.108	butylidenephthalide	$C_{12}H_{12}O_2$	189.0916	189.0902	−2.1	89.4471
2	$[M-H]+$	15.534	miltirone	$C_{19}H_{22}O_2$	283.1698	283.1684	−1.5	142.0888, 95.0618, 71.5483
3	$[M-H]+$	17.933	methylenetanshinquinone	$C_{18}H_{14}O_3$	279.1021	279.1025	0.3	140.0550, 93.7059, 70.5314
4	$[M-H]+$	22.727	tanshinone IIB	$C_{19}H_{18}O_4$	311.1283	311.1285	−0.9	156.0681, 104.3813, 78.5380
5	$[M-H]+$	23.648	senkyunolide A	$C_{12}H_{16}O_2$	193.1229	193.0388	−0.2	91.4061
6	$[M-H]+$	25.449	butylphthalide	$C_{12}H_{14}O_2$	191.1072	191.6543	0.6	145.7898
7	$[M-H]^-$	6.688	quinic acid	$C_7H_{12}O_6$	191.0556	191.0552	0.7	173.1321, 155.5332, 137.4562, 127.5325
8	$[M-H]^-$	21.950	apigenin-7-*O*-beta-*D*-glucoside	$C_{21}H_{20}O_{10}$	431.0978	431.0976	−0.6	341.2379, 311.4523, 269.0789
9	$[M-H]^-$	23.582	quercetin	$C_{15}H_{10}O_7$	301.0348	301.0340	−1.1	255.1255, 178.7645, 151.8732
10	$[M-H]^-$	23.855	salvianolic acid C	$C_{26}H_{20}O_{10}$	491.0978	491.1216	0.7	245.0450, 163.0274, 122.0186
11	$[M-H]^-$	24.097	salvianolic acid A	$C_{26}H_{22}O_{10}$	493.1135	493.1142	−0.3	313.8273, 295.8921
12	$[M-H]^-$	25.022	amentoflavone	$C_{30}H_{18}O_{10}$	537.0822	537.0828	−1.9	443.7832, 417.5301, 375.8928, 331.0233, 203.3428

hair growth was apparent in the positive group, but also suffered hair loss (Figure 2A). Hair growth scores showed a substantial decrease in the model group compared to the control group ($P < 0.001$), while those increased in all dose groups and the positive group in a time-dependent manner compared to the model group ($P < 0.001$), these results

https://doi.org/10.1021/acsomega.3c09648
ACS Omega 2024, 9, 10834−10851

Table 5. Compound Identification of Drug-Contained Plasma in Positive and Negative Ion Modes

peak (no.)	ion mode	R_t (min)	components name	molecular formula	measured mass (no.)	calculated mass (no.)	error (ppm)	MS/MS
1	[M − H]+	1.199	butylidenephthalide	$C_{12}H_{12}O_2$	189.0916	189.0902	−2.1	89.4471
2	[M − H]+	15.331	miltirone	$C_{19}H_{22}O_2$	283.1698	283.1684	−1.5	142.0888, 95.0618, 71.5483
3	[M − H]$^-$	21.950	apigenin-7-*O*-beta-D-glucoside	$C_{21}H_{20}O_{10}$	431.0978	431.0976	−0.6	269.0789
4	[M − H]$^-$	23.582	quercetin	$C_{15}H_{10}O_7$	301.0348	301.0340	−1.1	255.1255, 178.7645, 151.8732
5	[M − H]$^-$	23.855	salvianolic acid C	$C_{26}H_{20}O_{10}$	491.0978	491.1216	0.7	245.0450, 163.0274, 122.0186
6	[M − H]$^-$	24.097	salvianolic acid A	$C_{26}H_{22}O_{10}$	493.1135	493.1142	−0.3	313.8273, 295.8921
7	[M − H]$^-$	25.022	amentoflavone	$C_{30}H_{18}O_{10}$	537.0822	537.0828	−1.9	443.7832, 417.5301, 375.8928, 331.0233,203.3428

indicated the successful establishment of the AGA mouse model. Furthermore, it is noteworthy that all dose groups showed remarkable hair growth-promoting activity, suggesting that TSBHGD exerts a pronounced antialopecia effect in the AGA mouse model (Figure 2B,C).

3.2. Histological Observation of Skin in Hair Removal Areas. According to light microscopy examinations, the H&E staining of skin in hair removal areas is shown in Figure 3A,B. Histological analysis demonstrated that the hair follicles in the control group were actively proliferating with a larger number and diameter, and the formation of melanin was visible, while the model group indicated a significant reduction in dermal thickness and hair follicle counts. Compared to the model group, the density of hair follicles in all dose groups and the positive group increased significantly, along with the appearance of new hair follicles and inner root sheaths.

Compared to the model group, on day 7 after treatment, mice receiving minoxidil and high-dose TSBHGD had more hair follicles in the anagen phase ($P < 0.001$) and the control group had more hair follicles in the telogen phase ($P < 0.05$), whereas no significant changes in the remaining groups ($P > 0.05$) (Figure 3C). On day 14 after treatment, the control group ($P < 0.001$), the low-dose group ($P < 0.01$), the high-dose group ($P < 0.001$), and the positive group ($P < 0.001$) had more hair follicles in the anagen phase, whereas no significant changes in the telogen phase among groups (Figure 3D). Between days 7 and 14, the model group ($P < 0.05$) and the positive group ($P < 0.01$) had more hair follicles in the anagen phase and the positive group had more hair follicles in the telogen phase ($P < 0.05$), whereas no significant changes in the remaining group ($P > 0.05$) (Figure 3E).

3.3. Effects of TSBHGD on Inflammatory Factors TNF-α and IL-6. To reveal whether TSBHGD had anti-inflammatory effects, TNF-α and IL-6 levels of C57BL/6J mice were measured using ELISA kits. TNF-α and IL-6 levels in the model group increased remarkably compared to the control group ($P < 0.001$). Compared to the model group, the level of TNF-α in the high-dose group decreased remarkably ($P < 0.05$), while there was no significant change in the low-dose and positive groups ($P > 0.05$) (Figure 4A). Besides, the level of IL-6 in all dose groups decreased remarkably ($P < 0.01$), while there was no significant change in the positive group ($P > 0.05$) (Figure 4B). The results suggest that the development of AGA is accompanied by increased levels of inflammatory factors and topical application of TSBHGD can inhibit TNF-α and IL-6 levels.

3.4. TSBHGD Main Chemical Component Analysis. The base peak intensity (BPI) chromatograms of TSBHGD extracts in the positive and negative ion modes were collected by using the UPLC-Q-TOF-MS method (Figure 5A,B). This result demonstrated that the main components of the formula could be effectively separated under the abovementioned chromatographic conditions. The mass spectrometry data were compared with the local composition database, identifying 35 major components with clear chemical structures and relative peak areas >5%, including 13 organic acids, 8 flavonoids, 6 quinones, 5 coumarins, and 3 triterpenoid saponins. The results of the positive and negative ion scans are listed in Table 3.

3.5. Analysis of Skin-Retained and Blood-Retained Compounds in Mice after Topical Administration. The base peak chromatograms and mass spectrometry data of skin-retained and blood-retained components were collected using the optimized UPLC-Q-TOF-MS. The BPI chromatograms of drug-containing skin and drug-containing plasma in positive and negative ion modes are shown in Figures 6 and 7, respectively. Comparing the results with MS spectra, retention time, and fragmentation pattern to those of the corresponding TCMs and excluding the blank mass spectral signals indicated that 12 components were retained in the mouse skin, and 7 components were retained in the mouse blood, mainly organic acids and quinone compounds. Results of positive and negative ion patterns on the components retained in mouse skin and blood are shown in Tables 4 and 5, respectively.

3.6. PPI Network Construction. According to the outcomes of skin-retained and blood-retained components, the targets associated with these components were assembled by using the Swiss Target Prediction and STRING database. After the data from these databases were integrated, we obtained sufficient targets concerning the retained components. Then, Cytoscape V3.7.2 software was applied to compute topological parameters, such as "Degree" and construct PPI networks. The PPI network of skin-retained components included 203 nodes and 526 edges with a degree value ranging from 1 to 27, and the top ten targets were FYN, LYN, STAT3, YES1, HSP90AA1, FGR, BLK, PTPN11, SYK, ESR1 (Figure 8A). The PPI network of blood-retained components was composed of 238 nodes and 910 edges with a degree value ranging from 1 to 59. The top ten targets were identified based on the degree value, namely, SRC, PIK3R1, HSP90AA1, STAT3, FYN, LYN, LCK, PTK2, PTPN11, FGR (Figure 8B).

3.7. Sample Correlation Analysis. The mRNA profiles of genes in three distinct groups were examined using high-throughput sequencing technology: the control group, the AGA model group, and the high-dose TSBHGD group. Pearson's correlation analysis was conducted to assess the similarity and discrepancy among the three groups. The correlation coefficients of the three groups ranged from 0.9−1.0 for the control, 0.97−1.0 for the AGA model, and 0.94−

https://doi.org/10.1021/acsomega.3c09648
ACS Omega 2024, 9, 10834−10851

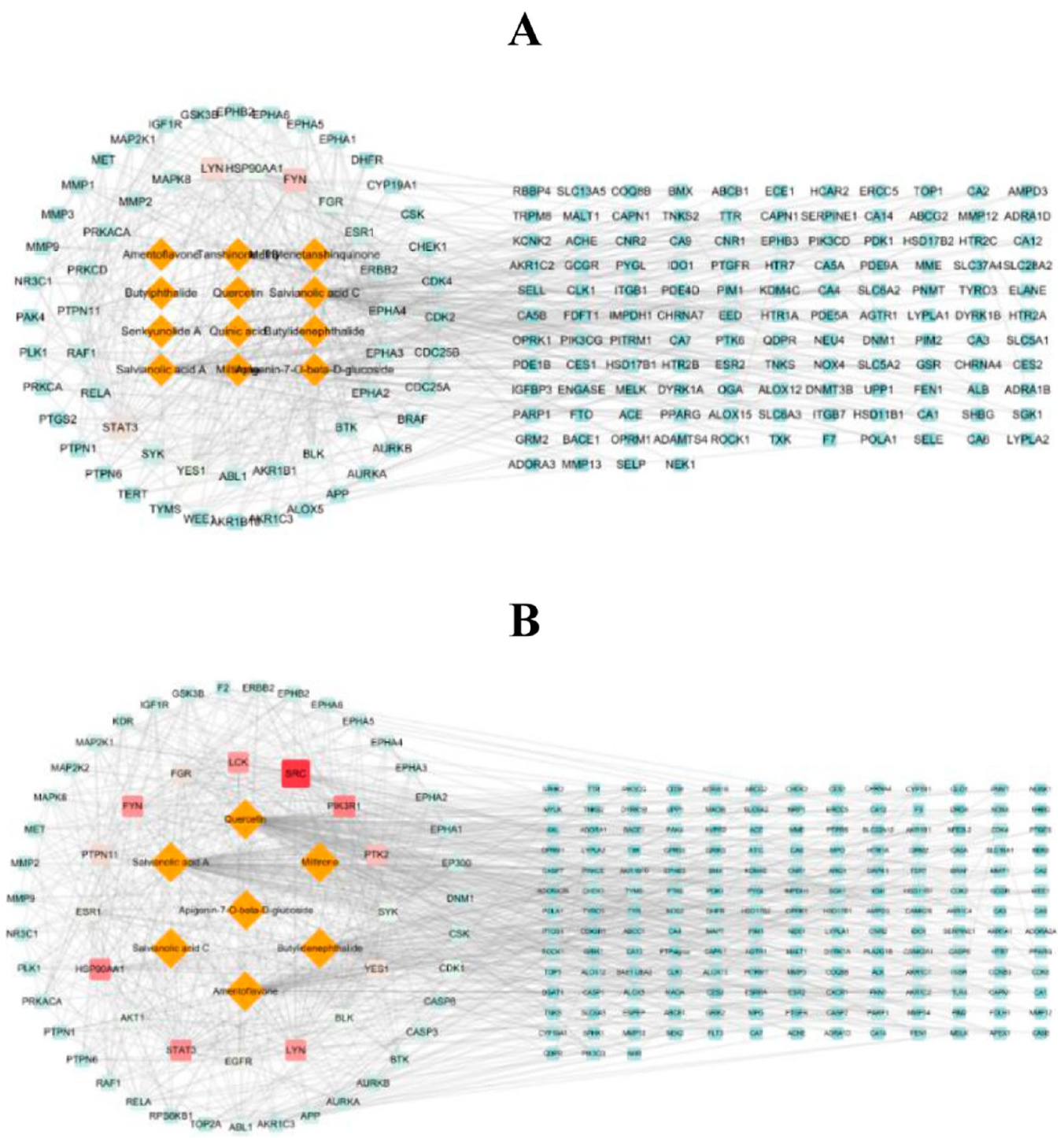

Figure 8. PPI network construction. (A) PPI network for potential targets of skin-retained components. (B) PPI network for potential targets of blood-retained components. The size and color of the targets increase with the value of "Degree" (blue, pink, and red in that order) and the orange diamonds in the middle represent the different drug components, respectively.

1.00 for high-dose TSBHGD (Figure 9A), suggesting that the samples within each group were highly correlated and revealing intergroup differences between the three groups from an overall perspective. PCA results showed that the first two PCs could explain 80.6% of gene expression variation (PC1: 62.5%, PC2: 18.1%), and the order of samples in this dimension was in the control, high-dose TSBHGD, and AGA model groups, suggesting that TSBHGD can reverse the altered gene expression patterns caused by androgen intervention to some extent (Figure 9B). The correlation heatmap and PCA analysis delineated distinct transcriptional signatures among the three groups, validating the high quality of RNA-seq data for subsequent analysis.

3.8. Differentially Expressed Genes. To investigate the mechanisms involved in promoting hair growth by TSBHGD treatment, we performed RNA-seq to investigate the genome-wide transcriptional changes in mice. Transcriptomic data were used to identify DEGs in the control vs AGA model with

https://doi.org/10.1021/acsomega.3c09648
ACS Omega 2024, 9, 10834−10851

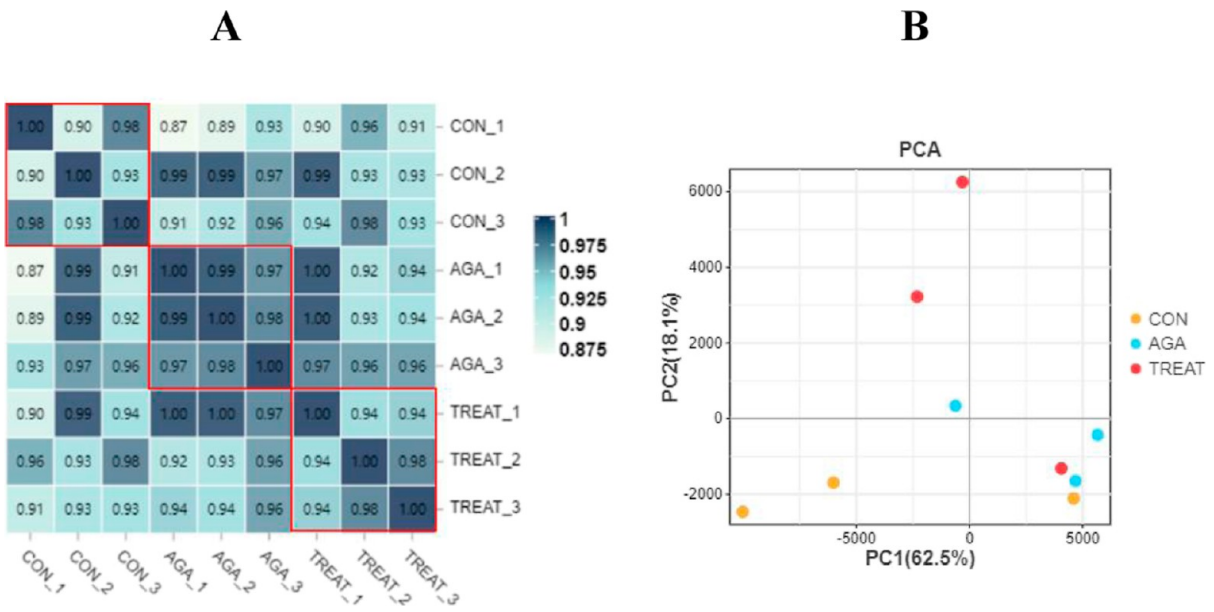

Figure 9. Correlation analysis between samples. (A) Pearson's correlation analysis was conducted to calculate logarithm-transformed counts for control, AGA model, and high-dose TSBHGD groups RNA-seq data set. (B) PCA analysis. PCA axis percentages indicate the proportion of variance explained by each PC. Control samples are marked in orange, AGA model samples are marked in blue, and high-dose TSBHGD samples are marked in red.

results of 94 including 67 genes upregulated and 27 genes downregulated, while AGA model vs high-dose TSBHGD with results of 145 including 128 genes upregulated and 17 genes downregulated (Figure 10A). In addition, PPI networks for DEGs were constructed and all node information was stored, and the PPI networks for control vs AGA model, and AGA model vs high-dose TSBHGD are shown in Figure 10B,C, respectively.

3.9. GO and KEGG Enrichment Analysis. Using the R V4.0.5 software setting adjusted *P*-value <0.01 and *Q*-value ≤0.05 in the programming language, the PPI network results of DEGs in the control vs AGA model and AGA model vs high-dose TSBHGD were intersected with that of human-derived targets in skin-retained and blood-retained components, giving a total of 85 key targets to form the gene set (Figure 11A). GO enrichment analysis of 85 potential targets was conducted through the Metascape database to obtain a total of 25 terms in the category BP, 2 in CC, and 13 in MF for target genes. The BP terms mainly involve cellular processes, biological regulation, response to stimuli, metabolic processes, and multicellular organismal processes. The CC terms mainly involve cellular anatomical entities and protein-containing complexes. The MF terms mainly involved catalytic activity, binding activity, structural molecule activity, transcriptional regulation activity, and molecular function regulator (Figure 11B). KEGG pathway enrichment analysis of potential target proteins was performed using the same database, and a total of 8 KEGG pathways were enriched in the four genomes shown in Figure 11C, PI3K-Akt, Apoptosis, Ras, Estrogen, Sphingolipid, TNF, Melanoma, and NF-κB, among which the apoptosis signaling pathway ranked first with a significance of 0.00149.

3.10. Effect of TSBHGD on Bcl-2 Family Proteins in the AGA Mouse Model. Subsequently, we investigated TSBHGD's effects on Bcl-2 family proteins' expression in the AGA mouse model. Compared to the control group, the levels of Bax ($P < 0.001$) and the Bax/Bcl-2 ratio ($P < 0.001$) were remarkably higher, while the level of Bcl-2 ($P < 0.001$) was remarkably lower in the model group, suggesting that the AGA mouse model was successfully modeled. Furthermore, compared to the model group, the levels of Bax ($P < 0.001$) and the Bax/Bcl-2 ratio ($P < 0.001$) were remarkably lower in all dose groups and the positive group, while the level of Bcl-2 was remarkably higher in the low-dose group ($P < 0.01$) and high-dose group ($P < 0.05$), and the positive group showed no significant change ($P > 0.05$), indicating that hair growth was improved (Figure 12). The results demonstrated that apoptosis levels were higher in the skin tissues of AGA mice than in the control group, and the topical application of TSBHGD and minoxidil could reduce apoptosis levels in the skin tissues of AGA mice and bring them back to normal.

3.11. Effect of TSBHGD on Caspase Family Proteins in the AGA Mouse Model. Finally, we investigated TSBHGD's effects on Caspase family proteins' expression in the AGA mouse model. Compared to the control group, the level of Caspase9 ($P > 0.05$) had no significant change, while the level of Caspase3 ($P < 0.05$) was remarkably higher in the model group. Compared to the model group, the level of Caspase9 was remarkably decreased in the low-dose group ($P < 0.001$), and the high-dose and the positive groups showed no significant change ($P > 0.05$) (Figure 13A,B). Furthermore, the level of Caspase3 was remarkably decreased in all dose groups and the positive group ($P < 0.001$) (Figure 13C,D).

4. DISCUSSION

Hair loss refers to the partial or total absence of hair on the scalp, and the main triggers for this condition include genetics, hormonal changes, medical conditions, medications, and environmental factors. Alopecia can be categorized into two fundamental types: scarring alopecia and nonscarring alopecia. Nonscarring alopecia is more frequently encountered in everyday life, whereas scarring alopecia is an infrequent variant characterized by compromised hair follicles, dermal scarring, and enduring hair loss.[20] AGA stands as the most prevalent contributor to nonscarring alopecia with variable severity,

https://doi.org/10.1021/acsomega.3c09648
ACS Omega 2024, 9, 10834−10851

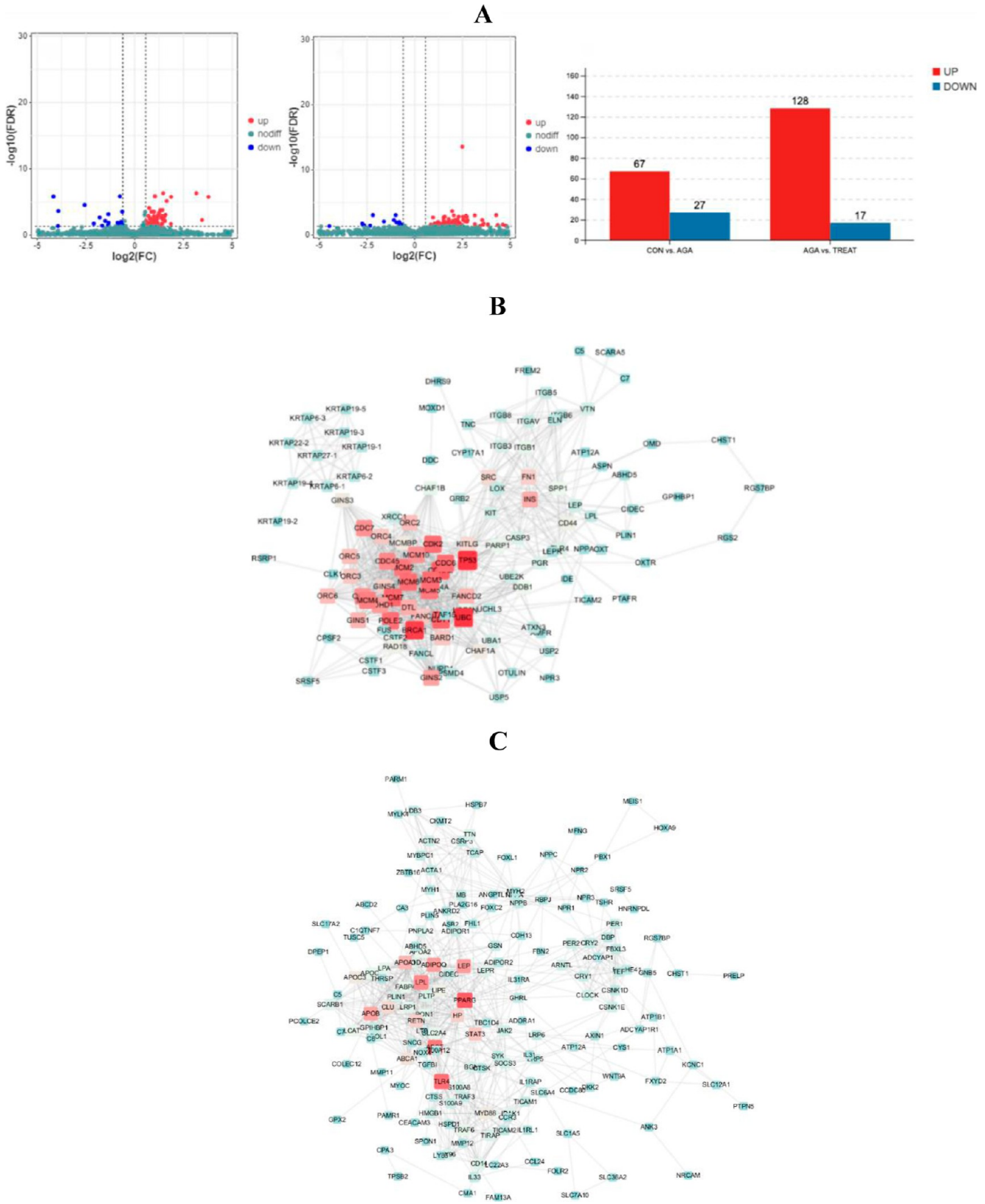

Figure 10. Differentially expressed genes. (A) Identification of DEGs in the control vs AGA model, AGA model vs high-dose TSBHGD, and summary of DEG numbers. (B) PPI network of DEGs of control vs AGA model. (C) PPI network of DEGs of the AGA model vs high-dose TSBHGD. The size and color of the targets increase with the value of "Degree" (blue, pink, and red in that order).

onset age, and scalp location of hair loss. Although the precise mechanism of AGA has not been fully determined, etiopathogenesis is generally attributed to aberrant androgen expression and impairments in androgen metabolism.[21] The androgen action on the hair follicle through the androgen receptor (AR) is thought to be the primary driver of follicle miniaturization

https://doi.org/10.1021/acsomega.3c09648
ACS Omega 2024, 9, 10834−10851

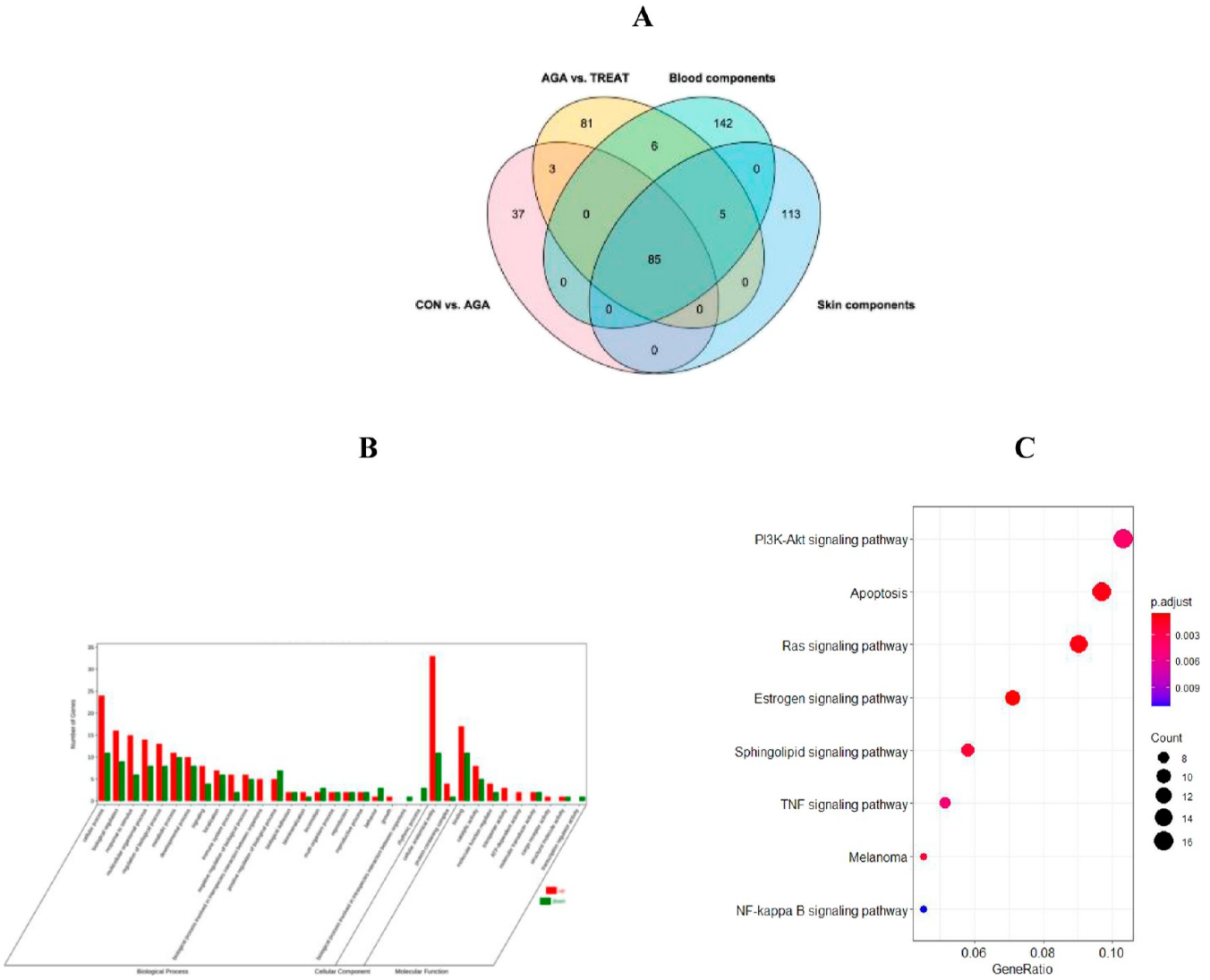

Figure 11. GO and KEGG Enrichment Analysis. (A) Intersection targets among the PPI network of DEGs in the control vs AGA model, AGA model vs high-dose TSBHGD, and that of human-derived targets in skin-retained and blood-retained components. (B) GO annotation for intersection targets of PPI in four groups. (C) KEGG annotation for intersection targets of PPI in four groups. The *x*-axis indicates the percentage of genes, the *y*-axis indicates the pathway, the size of the bubble indicates the pathway enrichment genes, and the color depth indicates the size of the *P*-value.

and the inhibition of hair growth in AGA.[22] Testosterone plays a central role among the circulating androgens, and its conversion to dihydrotestosterone (DHT) by the 5-AR enzyme represents a crucial element in the pathological mechanism of AGA,[23] DHT stands as the predominant causative androgen in AGA, resulting in hair follicle miniaturization and alterations in the cyclic phase.[24]

The hair-growth cycle comprises three distinct phases: the anagen (active growth), catagen (apoptosis-driven regression), and telogen (relatively stationary) observed in individual hair follicles.[25] One of the emblematic hair loss causes is the inability to regulate apoptosis during catagen, resulting in continued apoptotic induction.[26] The typical pathways of apoptosis are controlled by the proapoptotic Bcl-2 family: Bax, Bad, Bak, and the antiapoptotic Bcl-2 family: Bcl-2, Bcl-W, Bcl-XL.[27] The critical factor influencing apoptosis is the Bcl-2/Bax ratio, which declines significantly during the catagen phase in comparison to the anagen phase. Hence, elevating the Bcl-2/Bax ratio plays a pivotal role in preventing the transition from the anagen to the catagen phase.[28] In addition, the Caspase family proteins comprise a set of cysteine proteases that hold a pivotal function in the process of apoptosis. Activation of Caspase9 triggers a Caspase cascade reaction, which further activates downstream proteins, such as Caspase3, to cleave a variety of intracellular proteases, ultimately triggering apoptotic processes.[29] In China, many TCMs with historical heritage have been used for centuries to stimulate hair growth. Dou[30] revealed that monomeric components in TCMs can terminate or initiate a cascade of relevant factors by engaging a variety of pathways including PI3K/Akt, MAPKs, Wnt, Fas/FasL, and androgen receptor. In recent years, modern network pharmacology has played a pivotal role in explaining the potential mechanisms of TCMs in hair loss treatment, through diverse techniques such as network construction, visualization, and topology analysis.[31]

The C57BL/6 mouse is a widely used animal model for studying AGA, and the trunk skin of this mouse synthesizes melanin during the anagen phase and conveys it to keratin-

https://doi.org/10.1021/acsomega.3c09648
ACS Omega 2024, 9, 10834−10851

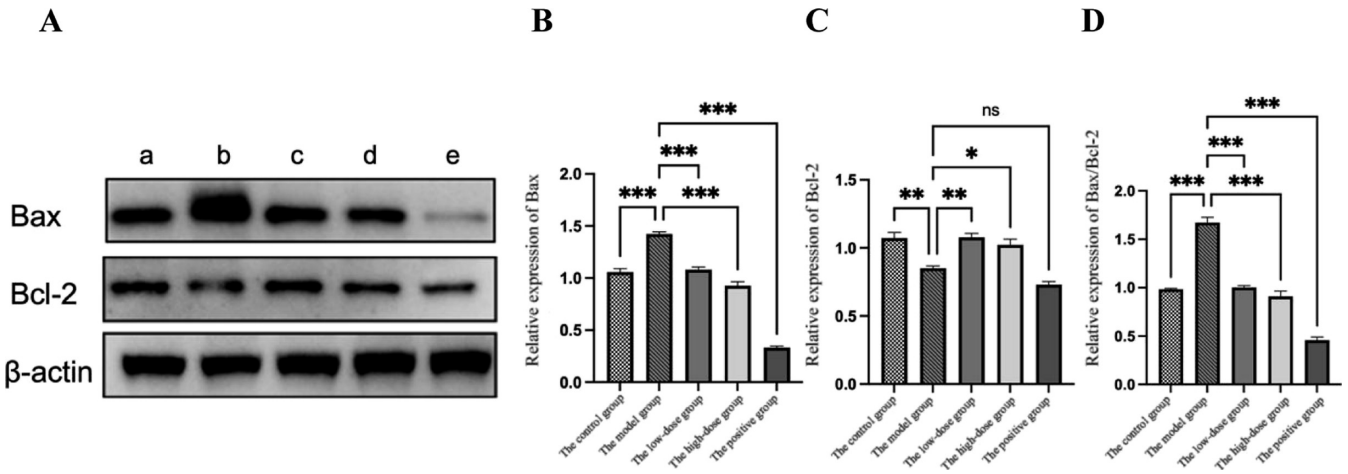

Figure 12. Effects of TSBHGD on Bcl-2 family protein expression in the skin tissue of each group. (A) Raw bands of Western Blot, where (a−e) represents the control group, model group, low-dose TSBHGD group, high-dose TSBHGD group, and positive group, respectively. (B) Relative expression of Bax. (C) Relative expression of Bcl-2. (D) Ratio of Bax/Bcl-2.

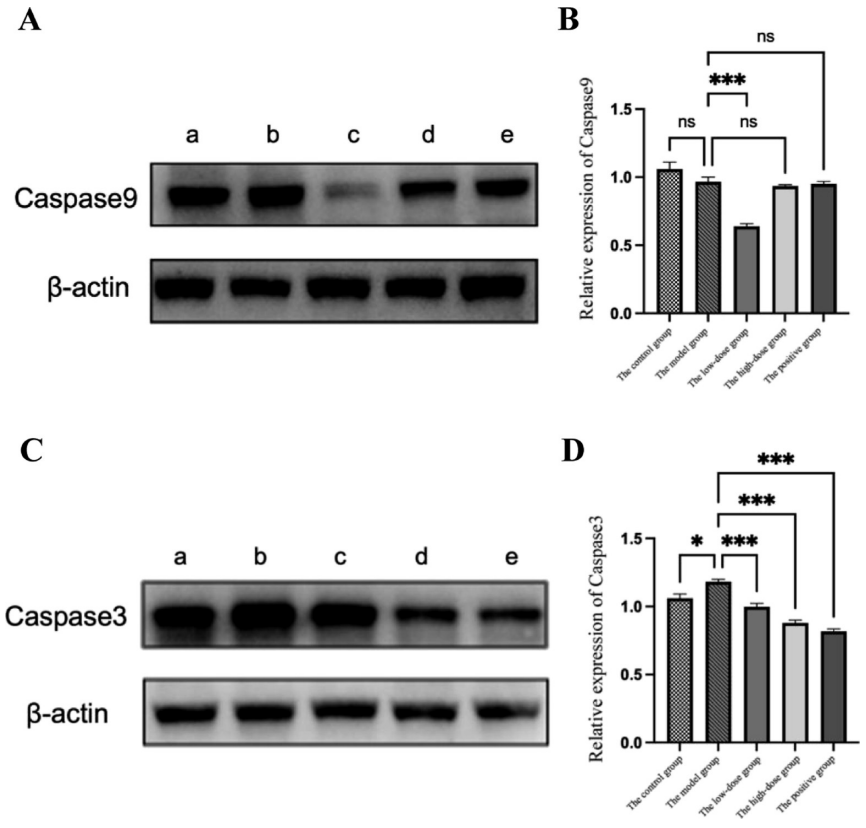

Figure 13. Effects of TSBHGD on Caspase family protein expression in the skin tissue of each group. (A) Raw bands of Caspase9 protein expression by Western Blot, where (ae) represents the control group, model group, low-dose TSBHGD group, high-dose TSBHGD group, and positive group, respectively. (B) Relative Expression of Caspase9. (C) Raw bands of Caspase3 protein expression by Western Blot, where a ∼ e represents the control group, model group, low-dose TSBHGD group, high-dose TSBHGD group, and positive group, respectively. (D) Relative expression of Caspase3.

forming cells, causing the skin to turn black, while the resting skin appears pink; therefore, the progression of the hair cycle can be determined based on skin color.[32] First, the AGA mouse model was replicated in C57BL/6J mice by applying testosterone solution, and the therapeutic effect of TSBHGD on AGA mice was investigated by using FDA-approved clinically used minoxidil as a positive drug, with hair growth scores, hair follicle counts in the anagen and telogen phases, histological determination, and TNF-α and IL-6 levels as evaluation indexes. The results demonstrated that TSBHGD could reduce TNF-α and IL-6 levels and improve pathological phenomena such as hair loss, reduced follicle density, and dermal thickness caused by testosterone solution, with a therapeutic effect close to that of minoxidil. Meanwhile, this study found that minoxidil had no modulating effect on inflammatory factors and hair follicle counts in the telogen

https://doi.org/10.1021/acsomega.3c09648
ACS Omega 2024, 9, 10834−10851

phase were significantly increased in AGA mice after 7−14 days of administration, which may be related to the clinical phenomenon of hair loss at the initial stage of the drug administration. Next, the TSBHGD extracts and the skin-retained and blood-retained components were qualitatively analyzed by UPLC-Q-TOF-MS. A total of 35 components were identified in the TSBHGD extracts, 12 skin-retained components were identified in the drug-containing skin, and 7 blood-retained components were identified in the drug-containing plasma, mainly organic acids and quinones. Furthermore, based on the human-derived targets of the skin and blood retention components, the PPI network was constructed to provide data support for further investigation of the mechanism of TSBHGD. Subsequently, to clarify the mechanism of TSBHGD, transcriptome sequencing was performed on the mice's skin tissues in the control vs AGA model and AGA model vs high-dose TSBHGD mice. The PPI network results of DEGs intersected with the PPI network results of human-derived targets in skin-retained components and blood-retained components, and a total of 85 key targets were obtained. GO and KEGG enrichment analyses revealed that the mechanism of TSBHGD was closely related to the apoptotic signaling pathway. Finally, the Bcl-2 and Caspase family proteins in the apoptosis signaling pathway were detected by Western Blot. The results showed that the levels of Bax, Bax/Bcl-2, and Caspase3 were remarkably increased, and the level of Bcl-2 was remarkably decreased in the model group compared to the control group. Compared to the model group, the levels of Bax, Bax/Bcl-2, Caspase3, and Caspase9 were remarkably lower, and the level of Bcl-2 was remarkably higher in the low-dose group; the levels of Bax, Bax/Bcl-2, and Caspase3 were remarkably lower, and the level of Bcl-2 was remarkably higher in the high-dose group; the levels of Bax, Bax/Bcl-2, and Caspase3 were remarkably lower in the positive group. These results confirmed that TSBHGD could inhibit the level of apoptosis in the skin tissues of AGA mice to exert an anti-AGA effect; the overall effect of apoptosis inhibition in the low-dose group was better than that in the high-dose group and minoxidil, and the increased dose did not inhibit apoptosis better.

Currently, the two FDA-approved hair growth agents have adverse effects, underscoring the pressing necessity for enhancing the safety and effectiveness of alternative treatments. In this study, we combined TCM theory with clinical treatment experience to develop an herbal compound formula consisting of seven TCMs, TSBHGD. Our results demonstrated that TSBHGD was more effective than minoxidil in promoting hair growth. In AGA mouse models, the topical application of TSBHGD induces hair follicles into the anagen phase to promote hair growth and may exert anti-AGA effects by improving the apoptotic protein expression levels of hair follicles. Furthermore, there was no erythema, redness, edema, drying, or scaling on the mice's dorsal skin after administration during the experiment, indicating that TSBHGD is a safe topical formulation that may be developed as a new-generation therapeutic remedy for AGA.

5. CONCLUSIONS

Drawing on the TCM theory and clinical treatment experience, we propose a novel compound formula, TSBHGD, to fill the gap in the TCM treatment of AGA. In this study, we evaluated the therapeutic effect of TSBHGD on AGA mice, analyzed the skin and blood retention components of TSBHGD, and tentatively clarified the pharmacological basis of its percutaneous absorption. Finally, we confirmed that TSBHGD could treat AGA by inhibiting the apoptosis levels in the mice's skin tissue. This advancement paves the way for the development of a novel herbal compound formula renowned for its effectiveness in AGA treatment, thereby presenting innovative prospects for TCM-based AGA therapy.

AUTHOR INFORMATION

Corresponding Authors

Yan Wang − *State Key Laboratory of Component-based Chinese Medicine, Tianjin University of Traditional Chinese Medicine, Tianjin 300193, China; Haihe Laboratory of Modern Chinese Medicine, Tianjin University of Traditional Chinese Medicine, Tianjin 300193, China; Tianjin University of Traditional Chinese Medicine, Tianjin 300193, China*; orcid.org/0000-0002-1757-513X; Email: wangyan@tjutcm.edu.cn

Beibei Xiang − *Tianjin University of Traditional Chinese Medicine, Tianjin 300193, China*; Email: xiangbeibei03230@163.com

Authors

Mingxi Li − *State Key Laboratory of Component-based Chinese Medicine, Tianjin University of Traditional Chinese Medicine, Tianjin 300193, China; Haihe Laboratory of Modern Chinese Medicine, Tianjin University of Traditional Chinese Medicine, Tianjin 300193, China; Tianjin University of Traditional Chinese Medicine, Tianjin 300193, China*

Xiujun Zhang − *Tianjin Academy of Traditional Chinese Medicine Affiliated Hospital, Tianjin 300120, China*

Zhaoyi Liu − *Tianjin University of Traditional Chinese Medicine, Tianjin 300193, China*

Wenwen Zhang − *Tianjin University of Traditional Chinese Medicine, Tianjin 300193, China*

Xuanming Liu − *Tianjin University of Traditional Chinese Medicine, Tianjin 300193, China*

Ruoxi Guo − *Tianjin Shangmei Cosmetics Co., Ltd, Tianjin 301617, China*

Complete contact information is available at: https://pubs.acs.org/10.1021/acsomega.3c09648

Author Contributions

M.L. and X.Z. contributed equally to this work and share first authorship. Data collection: M.L. and X.Z.; data analysis: M.L., Z.L., and W.Z.; experimental design: Y.W., B.X., and X.Z.; project design: Y.W., B.X., and R.G.; data interpretation and manuscript writing: M.L. and X.L.

Funding

This work was supported by the National Natural Science Foundation of China (grant number 81602773).

Notes

The authors declare no competing financial interest.

REFERENCES

(1) Premanand, A.; Reena Rajkumari, B. Androgen modulation of Wnt/β-catenin signaling in androgenetic alopecia. *Arch. Dermatol. Res.* **2018**, *310* (5), 391−399.

(2) Jain, R.; De-Eknamkul, W. Potential targets in the discovery of new hair growth promoters for androgenic alopecia. *Expert Opin. Ther. Targets* **2014**, *18* (7), 787−806.

https://doi.org/10.1021/acsomega.3c09648
ACS Omega 2024, 9, 10834−10851

(3) Wang, T. L.; Zhou, C.; Shen, Y. W.; Wang, X. Y.; Ding, X. L.; Tian, S.; Liu, Y.; Peng, G. H.; Xue, S. Q.; Zhou, J. E.; et al. Prevalence of androgenetic alopecia in China: a community-based study in six cities. *Br. J. Dermatol.* **2010**, *162* (4), 843−847.
(4) (a) Severi, G.; Sinclair, R.; Hopper, J. L.; English, D. R.; McCredie, M. R.; Boyle, P.; Giles, G. G. Androgenetic alopecia in men aged 40−69 years: prevalence and risk factors. *Br. J. Dermatol.* **2003**, *149* (6), 1207−1213. (b) Yip, L.; Zaloumis, S.; Irwin, D.; Severi, G.; Hopper, J.; Giles, G.; Harrap, S.; Sinclair, R.; Ellis, J. Gene-wide association study between the aromatase gene (CYP19A1) and female pattern hair loss. *Br. J. Dermatol.* **2009**, *161* (2), 289−294.
(5) Nestor, M. S.; Ablon, G.; Gade, A.; Han, H.; Fischer, D. L. Treatment options for androgenetic alopecia: Efficacy, side effects, compliance, financial considerations, and ethics. *J. Cosmet. Dermatol.* **2021**, *20* (12), 3759−3781.
(6) Tabolli, S.; Sampogna, F.; di Pietro, C.; Mannooranparampil, T. J.; Ribuffo, M.; Abeni, D. Health status, coping strategies, and alexithymia in subjects with androgenetic alopecia: a questionnaire study. *Am. J. Clin. Dermatol.* **2013**, *14* (2), 139−145.
(7) (a) Rossi, A.; Anzalone, A.; Fortuna, M. C.; Caro, G.; Garelli, V.; Pranteda, G.; Carlesimo, M. Multi-therapies in androgenetic alopecia: review and clinical experiences. *Dermatol. Ther.* **2016**, *29* (6), 424−432. (b) Adil, A.; Godwin, M. The effectiveness of treatments for androgenetic alopecia: A systematic review and meta-analysis. *J. Am. Acad. Dermatol.* **2017**, *77* (1), 136−141. (c) Gupta, A. K.; Mays, R. R.; Dotzert, M. S.; Versteeg, S. G.; Shear, N. H.; Piguet, V. Efficacy of non-surgical treatments for androgenetic alopecia: a systematic review and network meta-analysis. *J. Eur. Acad. Dermatol. Venereol.* **2018**, *32* (12), 2112−2125. (d) Gupta, A. K.; Cole, J.; Deutsch, D. P.; Everts, P. A.; Niedbalski, R. P.; Panchaprateep, R.; Rinaldi, F.; Rose, P. T.; Sinclair, R.; Vogel, J. E.; et al. Platelet-Rich Plasma as a Treatment for Androgenetic Alopecia. *Dermatol. Surg.* **2019**, *45* (10), 1262−1273. (e) Gupta, A. K.; Carviel, J. L. Meta-analysis of photobiomodulation for the treatment of androgenetic alopecia. *J. Dermatol. Treat.* **2021**, *32* (6), 643−647.
(8) Suchonwanit, P.; Iamsumang, W.; Leerunyakul, K. Topical finasteride for the treatment of male androgenetic alopecia and female pattern hair loss: a review of the current literature. *J. Dermatol. Treat.* **2022**, *33* (2), 643−648.
(9) (a) Ashique, S.; Sandhu, N. K.; Haque, S. N.; Koley, K. A Systemic Review on Topical Marketed Formulations, Natural Products, and Oral Supplements to Prevent Androgenic Alopecia: A Review. *Nat. Prod. Bioprospect.* **2020**, *10* (6), 345−365. (b) Padois, K.; Cantiéni, C.; Bertholle, V.; Bardel, C.; Pirot, F.; Falson, F. Solid lipid nanoparticles suspension versus commercial solutions for dermal delivery of minoxidil. *Int. J. Pharm.* **2011**, *416* (1), 300−304. (c) Sánchez-Díaz, M.; López-Delgado, D.; Montero-Vílchez, T.; Salvador-Rodríguez, L.; Molina-Leyva, A.; Tercedor-Sánchez, J.; Arias-Santiago, S. Systemic Minoxidil Accidental Exposure in a Paediatric Population: A Case Series Study of Cutaneous and Systemic Side Effects. *Journal of clinical medicine* **2021**, *10* (18), 4257.
(10) (a) Levy, L. L.; Emer, J. J. Female pattern alopecia: current perspectives. *Int. J. Women's Health* **2013**, *5*, 541−556. (b) Arias-Santiago, S.; Camacho-Martínez, F. M. Adverse Effects of 5-Alpha Reductase Inhibitor Therapy in Men With Androgenetic Alopecia: Is There Cause for Concern? *Actas Dermo-Sifiliogr.* **2016**, *107* (9), 709−711.
(11) Sadgrove, N. J. The new paradigm for androgenetic alopecia and plant-based folk remedies: 5α-reductase inhibition, reversal of secondary microinflammation and improving insulin resistance. *J. Ethnopharmacol.* **2018**, *227*, 206−236.
(12) Liang, Y.; Yuan, J.; Shazada, N. E.; Jiang, J.; Wu, J. Traditional Chinese Medicine Treatment for Androgenetic Alopecia Based on Animal Experiments: A Systematic Review and Meta-Analysis. *Evidence-Based Complementary Altern. Med.* **2022**, *2022*, 1−19.
(13) You, Q.; Li, L.; Ma, X.; Gao, T.; Xiong, S.; Yan, Y.; Fang, H.; Li, F.; Chen, H.; Liu, Y. Meta-Analysis on the Efficacy and Safety of Traditional Chinese Medicine as Adjuvant Therapy for Refractory Androgenetic Alopecia. *Evidence-Based Complementary Altern. Med.* **2019**, *2019*, 1−21.
(14) Dhariwala, M. Y.; Ravikumar, P. An overview of herbal alternatives in androgenetic alopecia. *J. Cosmet. Dermatol.* **2019**, *18* (4), 966−975.
(15) (a) Zhuang, B.; Bi, Z. M.; Wang, Z. Y.; Duan, L.; Lai, C. J.; Liu, E. H. Chemical profiling and quantitation of bioactive compounds in Platycladi Cacumen by UPLC-Q-TOF-MS/MS and UPLC-DAD. *J. Pharm. Biomed. Anal.* **2018**, *154*, 207−215. (b) Zhang, Y.; Chen, S.; Qu, F.; Su, G.; Zhao, Y. In vivo and in vitro evaluation of hair growth potential of Cacumen Platycladi, and GC-MS analysis of the active constituents of volatile oil. *J. Ethnopharmacol.* **2019**, *238*, 111835.
(16) Zhang, B.; Zhang, R. W.; Yin, X. Q.; Lao, Z. Z.; Zhang, Z.; Wu, Q. G.; Yu, L. W.; Lai, X. P.; Wan, Y. H.; Li, G. Inhibitory activities of some traditional Chinese herbs against testosterone 5α-reductase and effects of Cacumen platycladi on hair re-growth in testosterone-treated mice. *J. Ethnopharmacol.* **2016**, *177*, 1−9.
(17) Leem, J.; Jung, W.; Kim, Y.; Kim, B.; Kim, K. Exploring the combination and modular characteristics of herbs for alopecia treatment in traditional Chinese medicine: an association rule mining and network analysis study. *BMC Complementary Altern. Med.* **2018**, *18* (1), 204.
(18) (a) Choi, B. Y. Hair-Growth Potential of Ginseng and Its Major Metabolites: A Review on Its Molecular Mechanisms. *Int. J. Mol. Sci.* **2018**, *19* (9), 2703. (b) Lee, N. E.; Park, S. D.; Hwang, H.; Choi, S. H.; Lee, R. M.; Nam, S. M.; Choi, J. H.; Rhim, H.; Cho, I. H.; Kim, H. C.; et al. Effects of a gintonin-enriched fraction on hair growth: an in vitro and in vivo study. *J. Ginseng Res.* **2020**, *44* (1), 168−177.
(19) Abbas, A. N. Ginger (Zingiber officinale (L.) Rosc) improves oxidative stress and trace elements status in patients with alopecia areata. *Niger. J. Clin. Pract.* **2020**, *23* (11), 1555−1560.
(20) Alessandrini, A.; Bruni, F.; Piraccini, B. M.; Starace, M. Common causes of hair loss - clinical manifestations, trichoscopy and therapy. *J. Eur. Acad. Dermatol. Venereol.* **2021**, *35* (3), 629−640.
(21) Ceruti, J. M.; Leirós, G. J.; Balañá, M. E. Androgens and androgen receptor action in skin and hair follicles. *Mol. Cell. Endocrinol.* **2018**, *465*, 122−133.
(22) Inui, S.; Itami, S. Molecular basis of androgenetic alopecia: From androgen to paracrine mediators through dermal papilla. *J. Dermatol. Sci.* **2011**, *61* (1), 1−6.
(23) Said, M. A.; Mehta, A. The Impact of 5α-Reductase Inhibitor Use for Male Pattern Hair Loss on Men's Health. *Curr. Neurol. Rep.* **2018**, *19* (8), 65.
(24) (a) Dhurat, R.; Sharma, A.; Rudnicka, L.; Kroumpouzos, G.; Kassir, M.; Galadari, H.; Wollina, U.; Lotti, T.; Golubovic, M.; Binic, I.; et al. 5-Alpha reductase inhibitors in androgenetic alopecia: Shifting paradigms, current concepts, comparative efficacy, and safety. *Dermatol. Ther.* **2020**, *33* (3), No. e13379. (b) Grymowicz, M.; Rudnicka, E.; Podfigurna, A.; Napierala, P.; Smolarczyk, R.; Smolarczyk, K.; Meczekalski, B. Hormonal Effects on Hair Follicles. *Int. J. Mol. Sci.* **2020**, *21* (15), 5342.
(25) (a) Kim, M. H.; Choi, Y. Y.; Cho, I. H.; Hong, J.; Kim, S. H.; Yang, W. M. Angelica sinensis induces hair regrowth via the inhibition of apoptosis signaling. *Am. J. Chin. Med.* **2014**, *42* (4), 1021−1034. (b) Paus, R.; Cotsarelis, G. The biology of hair follicles. *N. Engl. J. Med.* **1999**, *341* (7), 491−497.
(26) Botchkareva, N. V.; Ahluwalia, G.; Shander, D. Apoptosis in the hair follicle. *J. Invest. Dermatol.* **2006**, *126* (2), 258−264.
(27) Kale, J.; Osterlund, E. J.; Andrews, D. W. BCL-2 family proteins: changing partners in the dance towards death. *Cell Death Differ.* **2018**, *25* (1), 65−80.
(28) Cho, E. C.; Kim, K. A comprehensive review of biochemical factors in herbs and their constituent compounds in experimental studies on alopecia. *J. Ethnopharmacol.* **2020**, *258*, 112907.
(29) Kim, M. H.; Choi, Y. Y.; Lee, J. E.; Kim, K.; Yang, W. M. Topical Treatment of Hair Loss with Formononetin by Modulating Apoptosis. *Planta Med.* **2016**, *82* (01/02), 65−69.
(30) Dou, J.; Zhang, Z.; Xu, X.; Zhang, X. Exploring the effects of Chinese herbal ingredients on the signaling pathway of alopecia and

https://doi.org/10.1021/acsomega.3c09648
ACS Omega 2024, 9, 10834−10851

the screening of effective Chinese herbal compounds. *J. Ethnopharmacol.* **2022**, *294*, 115320.
(31) Westerhoff, H. V. Network-based pharmacology through systems biology. *Drug Discovery Today: Technol.* **2015**, *15*, 15−16.
(32) (a) Ohn, J.; Kim, K. H.; Kwon, O. Evaluating hair growth promoting effects of candidate substance: A review of research methods. *J. Dermatol. Sci.* **2019**, *93* (3), 144−149. (b) Deng, Y.; Huang, F.; Wang, J.; Zhang, Y.; Zhang, Y.; Su, G.; Zhao, Y. Hair Growth Promoting Activity of Cedrol Nanoemulsion in C57BL/6 Mice and Its Bioavailability. *Molecules* **2021**, *26* (6), 1795.

https://doi.org/10.1021/acsomega.3c09648
ACS Omega 2024, 9, 10834−10851